On the use of a Darcy-Forchheimer like model for a macro-scale description of turbulence in porous media and its application to structured packings

Cyprien Soulaine, Michel Quintard

On the use of a Darcy–Forchheimer like model for a macro-scale description of turbulence in porous media and its application to structured packings

Cyprien Soulaine [a,*], Michel Quintard [a,b]

[a] Université de Toulouse, INPT, UPS, IMFT (Institut de Mécanique des Fluides de Toulouse), Allée Camille Soula, F-31400 Toulouse, France
[b] CNRS, IMFT, F-31400 Toulouse, France

A B S T R A C T

In this paper, we propose a methodology to derive a macro-scale momentum equation that is free from the turbulence model chosen for the pore-scale simulations and that is able to account for large-scale anisotropy. In this method, Navier–Stokes equations are first time-averaged to form a new set of equations involving an effective viscosity. The resulting balance equations are then up-scaled using a volume averaging methodology. This procedure gives a macro-scale generalized Darcy–Forchheimer equation to which is associated a closure problem that can be used to evaluate the apparent permeability tensor including inertia effects. This approach is validated through 2D and 3D calculations. Finally, the method is used to evaluate the tensorial macro-scale properties for a gas flow through structured packings.

Keywords:
Porous media
Volume averaging
Upscaling
Turbulence
Darcy–Forchheimer

1. Introduction

Structured packings play a large role in chemical engineering processes involving gas–liquid separation such as air distillation unit or CO_2 absorption columns [48,30]. Such structures maximize the exchange surface between gas and liquid while pressure drops remain low enough. Generally, the columns are operated in the counter-current flow mode: a thin liquid gravity film is sheared by the upward turbulent flow of a gas phase. We can apprehend such a structure as a high porosity porous medium for which the pore-scale is the elementary pattern that constitutes the structure packing while the macro-scale may be assimilated to the packing scale. Due to this structured geometry, the relationship between pressure drop within the packing and velocity may be anisotropic and may depend not only on the gas velocity but also on the flow direction. Moreover, gas can flow at very high pore-scale Reynolds number and the generated turbulence effects may lead to additional anisotropic behavior. In this paper we will assume that the liquid film is thin enough to have no significant impact on the gas pressure drop. Discussions regarding the liquid spreading in the structured packing are beyond the scope of this article. Readers that are concerned by such a topic can refer to the original approaches developed by Mahr and Mewes [22] and more recently revisited by Soulaine [47]. Consequently, we will only consider the gas flow.

Attempts to model three-dimensional gas flow patterns at the packing scale are still scarce in the chemical engineering literature. Mostly, the classical approach consists in empirical correlations based on one-dimensional Darcy–Forchheimer's law [4,49,3]. In these works, authors evaluated the Ergun's coefficients [15] as well as the exponent of the 1D Forchheimer inertial correction by fitting the pressure losses provided by laboratory-scale or industrial experiments. During the last decade, with the perspective of developing new types of column internal organs, researchers and manufacturers have used CFD simulations over a Representative Elementary Volume (REV) to evaluate the flow resistance in the direction of the column [34,42]. To account for the anisotropy induced from the structured packing geometry, Mewes et al. [26] introduced a flow resistance tensor that depends on the velocity magnitude. In the case of a packing made by corrugated sheets with an angle shift of 90° between two successive sheets, Raynal and Royon-Lebeaud [43] assume that the flow resistance in the horizontal axis is equivalent to the one calculated in the column vertical axis. From measurements and CFD simulations over cut-out segments of packing with different orientations, Mahr and Mewes [22] proposed correlations for the anisotropic gas flow resistance tensor as a function of direction and magnitude of the

* Corresponding author.
E-mail address: cyprien.soulaine@gmail.com (C. Soulaine).

Nomenclature

$\langle . \rangle^{\gamma}$	Intrinsic average for γ-phase
$\langle . \rangle$	Superficial average
ε_{γ}	Volume fraction of the γ-phase
V	Volume defining the unit-cell (m^3)
V_{γ}	Volume of the γ-phase within the unit-cell (m^3)
ρ_{γ}	Density in the γ-phase (kg/m^3)
$\mathbf{g}$	Gravity acceleration (m/s^2)
$\mathbf{v}_{\gamma}$	Velocity field in γ-phase i (m/s)
$\overline{\mathbf{v}}_{\gamma}$	Statistical average of $\mathbf{v}_{\gamma}$ (m/s)
$\langle \mathbf{v}_{\gamma} \rangle^{\gamma}$	Intrisic spatial average of $\overline{\mathbf{v}}_{\gamma}$ (m/s)
$\langle \mathbf{v}_{\gamma} \rangle$	Superficial spatial average of $\overline{\mathbf{v}}_{\gamma}$ (m/s)
$\tilde{\mathbf{v}}_{\gamma}$	Spatial deviation of $\overline{\mathbf{v}}_{\gamma}$ (m/s)
p_{γ}	Pressure field of the γ-phase ($kg/m/s^2$)
$\overline{p}_{\gamma}$	Statistical average of p_{γ} ($kg/m/s^2$)
$\overline{p}^{*}_{\gamma}$	Turbulent pressure ($kg/m/s^2$)
$\langle p_{\gamma} \rangle^{\gamma}$	Intrisic spatial average of$\overline{p}^{*}_{\gamma}$ ($kg/m/s^2$)
$\langle p_{\gamma} \rangle$	Superficial spatial average of $\overline{p}^{*}_{\gamma}$ ($kg/m/s^2$)
$\tilde{p}_{\gamma}$	Spatial deviation of $\overline{p}^{*}_{\gamma}$ ($kg/m/s^2$)
$\mu_{\gamma_{mol}}$	Molecular viscosity (kg/m/s)
$\mu_{\gamma_{turb}}(\mathbf{r})$	Turbulent viscosity (kg/m/s)
$\mu_{\gamma}(\mathbf{r}),\mu_{\gamma}$	Effective viscosity (kg/m/s)
$\langle \mu_{\gamma} \rangle^{\gamma}$	Intrisic spatial average of μ_{γ} ($kg/m/s^2$)
$\tilde{\mu}_{\gamma}$	Spatial deviation of μ_{γ} ($kg/m/s^2$)
k	Turbulent energy (m^2/s^2)
ϵ	Turbulent dissipation (m^2/s^3)
$C_1,C_2,C_{\mu},\sigma_k,\sigma_{\epsilon}$	closure variable of the $k-\epsilon$ model
l_{γ}	Characteristic length of the pore-scale (m)
L	Characteristic length of the macro-scale (m)
$Re_{\gamma_{turb}}$	Turbulent Reynolds number
Re	Reynolds number
$\mathbf{B}_{\gamma},\mathbf{B}^{0}_{\gamma}$	Closure variables
$\mathbf{b}_{\gamma},\mathbf{b}^{0}_{\gamma}$	Closure variables
$\mathbf{C}_{\gamma}$	Source term ($kg/m^3/s$)
$\mathbf{K}$	Permeability tensor (m^2)
$\mathbf{F}$	Forchheimer tensor
$\mathbf{K}^{*}$	Apparent permeability tensor (m^2)
$\frac{\Delta P}{L}$	Linear pressure drop ($kg/m^2/s^2$)

gas velocity. When increasing the mass flow rate, eddies are generated at the pore scale and accurate turbulent simulations must be performed. In such structures, the $k-\epsilon$ model is known to result in erroneous gas flow patterns and models that account for turbulent anisotropy such as the $k-\omega$ family are preferred [29,45,41,18]. However, all these approaches involving pore-scale turbulent CFD simulations attempt to predict the overall pressure loss in the industrial columns but not to determine the full anisotropic flow macro-properties.

Concerning the appropriate macro-scale model to be used in such cases, two major problems must be addressed. Firstly, it is not granted that a Darcy–Forchheimer's law is still acceptable for high pore-scale Reynolds numbers. Secondly, Direct Numerical Simulations (DNS) are not handy to analyze full anisotropic effects when local streamlines are deformed by inertial effects. Indeed, in the Darcy–Forchheimer regime, the inertia correction tensor depends not only on the medium but also on both Reynolds number and pressure gradient orientation [20]. This means that to a local velocity field corresponds a full Forchheimer tensor, *i.e.*, we have potentially 9 unknowns for only 3 equations if one assumes that the permeability tensor has been previously estimated. DNS alone cannot provide informations for all the tensor coefficients and that is why computation through closure problems are preferred [52]. Let us examine the first problem. Indeed, the question of turbulence modeling in porous media remains a challenging field of study and has not received a complete, comprehensive theoretical solution. Experimental investigations [9] performed over simple and complex porous media are in favor of a Darcy–Forchheimer model (the superficial velocity is non-linearly related to the pressure drop according to a function that depends on the solid structure and a power of the Reynolds number that varies between 0 and 1), even in the case of pore-scale turbulence. Moreover, most of the empirical correlations that evaluate the overall dry pressure drop of distillation columns [4,49,3]are based on such a formalism. Kuwahara et al. [19] conducted numerical experiments for turbulent flows through a periodic array of square cylinders using Large Eddy Simulations (LES). They showed that, in such case, Darcy–Forchheimer equation may well predict the pressure losses. From a purely theoretical point of view, numerous attempts to model turbulence effects in porous media have emerged in the literature this last decade. One can find an exhaustive review in [10,11]. Basically, two opposite approaches can be found concerning the derivation of macro-scale equations that model turbulence in a porous medium: either the use of volume averaging operator before time averaging is applied [1,17]or the application of time averaging followed by volume averaging [24,28,27,35,7,12]. Using the double decomposition concept introduced in [32,33]demonstrated that these two approaches should be mathematically equivalent, i.e., the two additional viscous and drag terms in the momentum balance equation have identical final forms after the application of both operators. Defining a macro-scale turbulent kinetic energy and a macroscopic turbulent viscosity, authors propose $k-\epsilon$ models with additional resistance terms due to the porous structure. The turbulent kinetic energy is used to evaluate the level of turbulence and thus a diffusion term in the momentum equation. This diffusion term is non-zero only when the gradient of the volume averaged velocity is non-zero, usually close to a free fluid domain [5] or a singular object which generates extra-pore eddies at larger scales. This kind of situation may also occur in some "porous media" with high porosity and permeability, for the investigation of forest fire spreading [36], of flows in electric cupboards or wind flows within an high density city for example. This concept is relevant when one studies the transition of a turbulent flow from a free domain towards a porous medium, since it provides a continuity of the turbulent variables [6]. However, in many cases, turbulence effects are confined to the intra-pore domains. This is for example the case for high Reynolds number flows in structured packing (see Fig. 6): vapor streams flow through each "channel" and eddies are generated at each criss-crossing junction and remain confined in this area which will prevent the appearance of large scale eddies. In such case, we suppose that macro-scale models involving turbulent kinetic energy are no longer necessary to model high velocity flows in porous media, and, possibly as we shall demonstrate, Darcy–Forchheimer type-like models offer a convenient way of representing the macro-scale behavior.

In this paper, we derive a macro-scale model that accounts for pore-scale turbulence. In the proposed method, Navier–Stokes equations are classically first time-averaged to form a new set of equations involving an effective viscosity. The resulting balance equations are then up-scaled in a restrictive sense developed later in this paper, using the volume averaging methodology as depicted in [53]. It yields a generalized Darcy–Forchheimer law where

effective parameters results from pore-scale simulations. This approach is then validated through 2D and 3D calculations. Finally, we apply the method to evaluate the *tensorial* macro properties of gas flow through examples of structured packings.

2. Pore-scale problem

The following development considers the flow of an incompressible single-phase (denoted γ-phase) in a saturated, rigid porous medium where the solid phase is denoted σ. If the time and space mesh scales are small enough to represent all the flow patterns, including turbulence, then the Navier–Stokes equations may be used to simulate the flow through the solid structure

$$\nabla \cdot \mathbf{v}_\gamma = 0 \text{ in } V_\gamma, \tag{1}$$

$$\rho_\gamma \frac{\partial \mathbf{v}_\gamma}{\partial t} + \rho_\gamma \mathbf{v}_\gamma \cdot \nabla \mathbf{v}_\gamma = -\nabla p_\gamma + \rho_\gamma \mathbf{g} + \nabla \cdot (\mu_{\gamma_{mol}} \nabla \mathbf{v}_\gamma) \text{ in } V_\gamma, \tag{2}$$

$$\mathbf{v}_\gamma = \mathbf{0} \text{ at } \mathcal{A}_{\sigma\gamma}, \tag{3}$$

where $\rho_\gamma, \mathbf{v}_\gamma, p_\gamma, \mathbf{g}$ and $\mu_{\gamma_{mol}}$ respectively stand for the fluid density, the velocity, the pressure field, the gravity and the molecular viscosity.

Up-scaling of this pore-scale problem has received a lot of attention in the literature. It has already been shown that the volume averaging of such a system at moderate Reynolds numbers leads to a Darcy–Forchheimer equation [52], in which the Forchheimer correction is not necessarily of the quadratic type, as previously suggested empirically by Forchheimer [16]. Indeed, it has been found that the first correction to Darcy's law, i.e., very small Reynolds number for classical porous media, is of cubic type [55] using asymptotic homogenization and on the basis of numerical simulations by Barrère [2]. Subsequent investigations taking into account larger Reynolds numbers suggested various dependence for the Forchheimer correction [46,20]. The work of Lasseux et al. [20] shows that these different behaviors can be retrieved following the derivation in [52], i.e., under the form of a generalized Darcy–Forchheimer equation. Here the word "generalized" emphasizes the fact that the correction is not necessarily of the quadratic type, and we will come back on this notion at the end of the paper. However, in the case of turbulent regimes, Direct Numerical Simulations of the Navier–Stokes equations would require very small mesh sizes and time steps, which is often inaccessible because of heavy computer resources requirements. This has called for the development of turbulence models as discussed below.

Many turbulence models have been developed. A typical example is the Reynolds Averaged Navier–Stokes (RANS) model (see one of the the numerous books on the topic as Wilcox [54] for example). This approach consists to time-average the Navier–Stokes equations (1)–(3). These equations are then transformed using the Reynolds decomposition of each field into the time-averaged contribution and a fluctuating quantity. The resulting equations involve more unknown variables (essentially in the term called the Reynolds stress tensors) than equations and consequently a closure is needed. The Boussinesq approximation introduces the eddy diffusivity concept to model the Reynolds stress tensor resulting from the time-averaging operation. All the RANS turbulence models ($k-\epsilon, k-\omega \ldots$) attempt to evaluate this new viscosity using extra transport equations to represent the turbulent properties of the flow.

For example, the "Standard" $k-\epsilon$ model [21], which is one of the most common turbulence models, adds to the Reynolds averaged momentum and continuity equations two additional equations to account for effects like convection and diffusion of turbulent energy. The first variable is the turbulent kinetic energy k and the second one is the turbulent dissipation ϵ. This latter variable determines the rate at which turbulence kinetic energy is converted into thermal internal energy, whereas the first variable determines the turbulence energy. This model is formulated as

$$\nabla \cdot \overline{\mathbf{v}}_\gamma = 0 \text{ in } V_\gamma, \tag{4}$$

$$\rho_\gamma \left(\frac{\partial \overline{\mathbf{v}}_\gamma}{\partial t} + \overline{\mathbf{v}}_\gamma \cdot \nabla \overline{\mathbf{v}}_\gamma \right) = -\nabla \left(\overline{p}_\gamma + \frac{2}{3}\rho k \right) + \rho_\gamma \mathbf{g} + \nabla \cdot \left(\left(\mu_{\gamma_{mol}} + \mu_{\gamma_{turb}}(\mathbf{r}) \right) \nabla \overline{\mathbf{v}}_\gamma \right) \text{ in } V_\gamma, \tag{5}$$

$$\rho_\gamma \left(\frac{\partial k}{\partial t} + \overline{\mathbf{v}}_\gamma \cdot \nabla k \right) = \nabla \cdot \left(\left(\mu_{\gamma_{mol}} + \frac{\mu_{\gamma_{turb}}(\mathbf{r})}{\sigma_k} \right) \nabla k \right) + \mu_{\gamma_{turb}}(\mathbf{r}) \nabla \overline{\mathbf{v}}_\gamma : \nabla \overline{\mathbf{v}}_\gamma - \rho_\gamma \epsilon \text{ in } V_\gamma, \tag{6}$$

$$\rho_\gamma \left(\frac{\partial \epsilon}{\partial t} + \overline{\mathbf{v}}_\gamma \cdot \nabla \epsilon \right) = \nabla \cdot \left(\left(\mu_{\gamma_{mol}} + \frac{\mu_{\gamma_{turb}}(\mathbf{r})}{\sigma_\epsilon} \right) \nabla \epsilon \right) + C_1 \frac{\epsilon^2}{k} \mu_{\gamma_{turb}}(\mathbf{r}) \nabla \overline{\mathbf{v}}_\gamma : \nabla \overline{\mathbf{v}}_\gamma - \rho_\gamma C_2 \frac{\epsilon^2}{k} \text{ in } V_\gamma. \tag{7}$$

In these equations, the overlines depict the statistical averaged quantities. The turbulent viscosity is then evaluated from the k and ϵ values through the relation

$$\mu_{\gamma_{turb}}(\mathbf{r}) = \rho_\gamma C_\mu \frac{k^2}{\epsilon}. \tag{8}$$

This system of equations requires some additional values to be entirely closed. A common set of values is [54]: $C_\mu = 0.09$; $C_1 = 1.44$; $C_2 = 1.92$; $\sigma_k = 1$; $\sigma_\epsilon = 1$.

Some authors (see [28,27,35,12] for instance) attempt to volume average this set of equations in order to propose a macroscopic version of the $k-\epsilon$ turbulence model in porous media. However, their methods are fully dependent of the chosen model for the microscopic calculations, i.e., the $k-\epsilon$ model. The developments should be carried on again if one wishes to up-scale one of the numerous versions of the $k-\epsilon$ or a $k-\omega$ SST model.

In this paper, we propose a complementary and original approach assuming that all the turbulence properties required to fully represent the flow are incorporated within the variable viscosity $\mu_\gamma(\mathbf{r})$ resulting from turbulent simulations at the scale of the REV. In this analysis, we do not take into consideration the energy and dissipation equations, which brings an important simplification to the problem that will allow us to investigate more deeply anisotropic effects by up-scaling only the momentum and continuity equations (this time with a spatially variable viscosity). Hence, the mathematical boundary value problem can be summed up as

$$\nabla \cdot \overline{\mathbf{v}}_\gamma = 0 \text{ in } V_\gamma, \tag{9}$$

$$\rho_\gamma \frac{\partial \overline{\mathbf{v}}_\gamma}{\partial t} + \rho_\gamma \overline{\mathbf{v}}_\gamma \cdot \nabla \overline{\mathbf{v}}_\gamma = -\nabla \overline{p}^*_\gamma + \rho_\gamma \mathbf{g} + \nabla \cdot (\mu_\gamma(\mathbf{r}) \nabla \overline{\mathbf{v}}_\gamma) \text{ in } V_\gamma, \tag{10}$$

$$\overline{\mathbf{v}}_\gamma = 0 \text{ at } \mathcal{A}_{\sigma\gamma}. \tag{11}$$

Here we have introduced the notion of turbulent pressure such as $\overline{p}^*_\gamma = \overline{p}_\gamma + \frac{2}{3}k$.

It is important to notice that all RANS models can be written following such a formulation. We also note that, despite a different origin of the derivation, the momentum equation in Large Eddy Simulations (LES) models can also be written under this effective viscosity formulation. In short, the approach we will develop in the next sections offers a general framework to *interpret* turbulent simulations in porous media in terms of a macro-scale model. Once again, we insist on the fact that the usefulness of the approach relies on the obtention of local quasi-periodic turbulent fields and

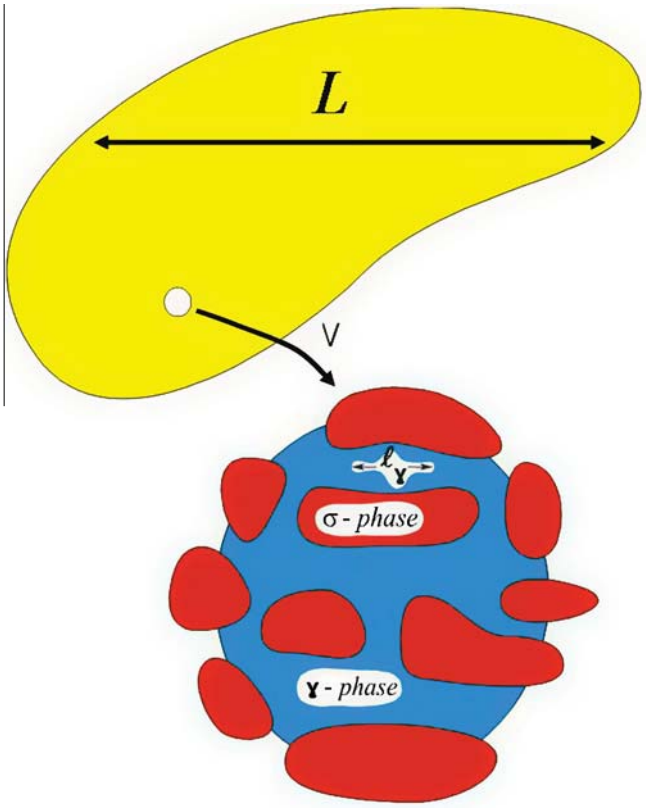

Fig. 1. Schematic representation of the hierarchy of length scales of a model porous medium and of a typical representative volume. This figure illustrates the three characteristic length-scales involved in this system: (1) the macro-scale, L; (2) the radius of the averaging volume, R; and (3) the average pore size, l_γ. Throughout this paper we use the following assumption: $l_\gamma \ll R \ll L$.

that the following developments are free from the turbulence model chosen for the pore-scale simulations.

3. Volume averaging

The problem formed by Eqs. (9)–(11) is reminiscent of the problem studied in [52] with the additional difficulty that viscosity varies in space. Therefore, we will follow the lines of development of this paper, with the necessary modifications. We will not detail all steps relevant to the volume averaging procedure and we refer the reader to the literature, for instance to [53], for further general details. We recall in this section the main definitions and theorems necessary to develop the macroscopic model from the pore-scale equations using the volume averaging methodology. We consider the averaging volume as illustrated in Fig. 1.

For a tensor ψ_γ (order 0, 1 or 2) associated with the γ-phase, we define the superficial average as

$$\langle \psi_\gamma \rangle = \frac{1}{V} \int_{V_\gamma} \psi_\gamma dV \tag{12}$$

and the corresponding intrinsic phase average as

$$\langle \psi_\gamma \rangle^\gamma = \frac{1}{V_\gamma} \int_{V_\gamma} \psi_\gamma dV. \tag{13}$$

Both are connected by

$$\langle \psi_\gamma \rangle = \varepsilon_\gamma \langle \psi_\gamma \rangle^\gamma \text{ with } \varepsilon_\gamma = \frac{V_\gamma}{V}, \tag{14}$$

where V_γ is the volume of the γ-phase and ε_γ is the porosity of the medium. Throughout this paper, the porous medium is homogeneous and ε_γ does not vary.

The phase variable ψ_γ is classically expressed using the following decomposition

$$\psi_\gamma = \langle \psi_\gamma \rangle^\gamma + \tilde{\psi}_\gamma. \tag{15}$$

Further, from Eqs. (15) and (12) we approximatively have

$$\langle \tilde{\psi}_\gamma \rangle \simeq 0. \tag{16}$$

To interchange integrals and derivatives, we will use the following two theorems [23]. For spatial averaging, we have

$$\langle \nabla \psi_\gamma \rangle = \nabla \langle \psi_\gamma \rangle + \frac{1}{V} \int_{\mathcal{A}_{\gamma\sigma}} \mathbf{n}_{\gamma\sigma} \psi_\gamma d\mathcal{A}, \tag{17}$$

for the gradient operator and a similar expression for the divergence operator. The integrals in this equality express the interfacial effects typical of porous media physics. For time derivatives, direct application of the Reynolds transport theorem for *static* boundaries yields

$$\left\langle \frac{\partial \psi_\gamma}{\partial t} \right\rangle = \frac{\partial \langle \psi_\gamma \rangle}{\partial t}. \tag{18}$$

3.1. Continuity equation

The mere application of the volume averaging theorem Eq. (17) to the continuity equation (9) leads to

$$\nabla . \langle \mathbf{v}_\gamma \rangle + \frac{1}{V} \int_{\mathcal{A}_{\gamma\sigma}} \mathbf{n}_{\gamma\sigma} \cdot \mathbf{v}_\gamma d\mathcal{A} = 0. \tag{19}$$

Moreover, from the no-slip velocity boundary condition at the fluid–solid interface and the relation equation (14), we deduce that

$$\nabla . \langle \mathbf{v}_\gamma \rangle^\gamma = 0. \tag{20}$$

Note that, for sake of clarity, we have removed the overline notations that depict the time-averaged values. The reader must keep in mind that the pressure and velocity fields considered in the rest of the development are in reality time-averaged fields.

3.2. Momentum conservation

We now form the averaged momentum balance equation by successive applications of the volume averaging theorem. We start from the conservative form of Eq. (10) for the γ-phase

$$\underbrace{\frac{\partial \rho_\gamma \mathbf{v}_\gamma}{\partial t} + \nabla \cdot \left(\rho_\gamma \mathbf{v}_\gamma \mathbf{v}_\gamma \right)}_{(LHS)} = \underbrace{-\nabla p_\gamma + \rho_\gamma \mathbf{g} + \nabla \cdot \left(\mu_\gamma(\mathbf{r}) \nabla \mathbf{v}_\gamma \right)}_{(RHS)} \quad \text{in } V_\gamma. \tag{21}$$

We remind the reader that, in this equation, the velocity and pressure fields are time averaged and that we have defined an effective viscosity $\mu_\gamma(\mathbf{r})$ that combines both molecular ($\mu_{\gamma_{mol}}$) and turbulent ($\mu_{\gamma_{turb}}(\mathbf{r})$) viscosities. This latter viscosity is a known field obtained from micro-scale turbulent simulations. Hence, in our analysis, $\mu_\gamma(\mathbf{r})$ is an input scalar field that may strongly vary within the REV.

The average of the left hand side leads to

$$\langle LHS \rangle = \frac{\partial \rho_\gamma \langle \mathbf{v}_\gamma \rangle}{\partial t} + \nabla \cdot \left(\rho_\gamma \langle \mathbf{v}_\gamma \mathbf{v}_\gamma \rangle \right) \tag{22}$$

and, with the decomposition $\mathbf{v}_\gamma = \langle \mathbf{v}_\gamma \rangle^\gamma + \tilde{\mathbf{v}}_\gamma$ and $\langle \mathbf{v}_\gamma \rangle = \varepsilon_\gamma \langle \mathbf{v}_\gamma \rangle^\gamma$, it becomes

$$\langle LHS \rangle = \frac{\partial \varepsilon_\gamma \rho_\gamma \langle \mathbf{v}_\gamma \rangle^\gamma}{\partial t} + \nabla \cdot \left(\varepsilon_\gamma \rho_\gamma \langle \mathbf{v}_\gamma \rangle^\gamma \langle \mathbf{v}_\gamma \rangle^\gamma \right) + \nabla \cdot \left(\rho_\gamma \langle \tilde{\mathbf{v}}_\gamma \tilde{\mathbf{v}}_\gamma \rangle \right), \tag{23}$$

using the macroscopic continuity equation (20) it can be transformed to a non-conservative form:

$$\langle LHS\rangle = \varepsilon_\gamma \rho_\gamma \frac{\partial \langle \mathbf{v}_\gamma\rangle^\gamma}{\partial t} + \varepsilon_\gamma \rho_\gamma \langle \mathbf{v}_\gamma\rangle^\gamma \cdot \nabla \langle \mathbf{v}_\gamma\rangle^\gamma + \nabla \cdot (\rho_\gamma \langle \tilde{\mathbf{v}}_\gamma \tilde{\mathbf{v}}_\gamma\rangle). \tag{24}$$

We continue the development with the averaging of the right hand side. This part is close to the derivation of Darcy's law from the Stokes problem proposed by Whitaker [51] and extensively presented in other works [38–40,50]. Since, in our analysis, we account for a variable viscosity, the derivation of the averaged equation from the micro-scale problem is, however, a little bit different than usual. The application of the volume averaging theorem Eq. (17) gives

$$\langle RHS\rangle = -\nabla\langle p_\gamma\rangle - \frac{1}{V}\int_{\mathcal{A}_{\gamma\sigma}} \mathbf{n}_\gamma p_\gamma d\mathcal{A} + \langle \rho_\gamma \mathbf{g}\rangle + \nabla\cdot\langle \mu_\gamma \nabla \mathbf{v}_\gamma\rangle + \frac{1}{V}\int_{\mathcal{A}_{\gamma\sigma}} \mathbf{n}_{\gamma\sigma}\cdot\mu_\gamma\nabla\mathbf{v}_\gamma d\mathcal{A}. \tag{25}$$

In this relation we can note that

$$\langle \mu_\gamma \nabla \mathbf{v}_\gamma\rangle = \varepsilon_\gamma \langle \mu_\gamma\rangle^\gamma \nabla\langle \mathbf{v}_\gamma\rangle^\gamma + \langle \mu_\gamma \nabla \tilde{\mathbf{v}}_\gamma\rangle \tag{26}$$

and

$$\frac{1}{V}\int_{\mathcal{A}_{\gamma\sigma}} \mathbf{n}_{\gamma\sigma}\cdot\mu_\gamma\nabla\mathbf{v}_\gamma d\mathcal{A} = \langle\nabla\tilde{\mu}_\gamma\rangle\cdot\nabla\langle\mathbf{v}_\gamma\rangle^\gamma - \langle\mu_\gamma\rangle^\gamma\nabla\langle\mathbf{v}_\gamma\rangle^\gamma\cdot\nabla\varepsilon_\gamma + \frac{1}{V}\int_{\mathcal{A}_{\gamma\sigma}} \mathbf{n}_{\gamma\sigma}\cdot\mu_\gamma\nabla\tilde{\mathbf{v}}_\gamma d\mathcal{A}, \tag{27}$$

where we have used the relation,

$$\frac{1}{V}\int_{\mathcal{A}_{\gamma\sigma}} \mathbf{n}_{\gamma\sigma}\tilde{\mu}_\gamma d\mathcal{A} = \langle\nabla\tilde{\mu}_\gamma\rangle. \tag{28}$$

We search an averaged equation in terms of the intrinsic average velocity and pressure $\langle\mathbf{v}_\gamma\rangle^\gamma$ and $\langle p_\gamma\rangle^\gamma$. Using the spatial decomposition, Eq. (15) for $\mathbf{v}_\gamma$ and p_γ and the relation equation 14 that relates intrinsic and superficial averages, one can eventually obtain:

$$\begin{aligned}\langle RHS\rangle = &-\varepsilon_\gamma\nabla\langle p_\gamma\rangle^\gamma + \varepsilon_\gamma\rho_\gamma\mathbf{g} + \varepsilon_\gamma\nabla\cdot(\langle\mu_\gamma\rangle^\gamma\nabla\langle\mathbf{v}_\gamma\rangle^\gamma) + \nabla\\ &\cdot\langle\mu_\gamma\nabla\tilde{\mathbf{v}}_\gamma\rangle + \langle\nabla\tilde{\mu}_\gamma\rangle\cdot\nabla\langle\mathbf{v}_\gamma\rangle^\gamma + \frac{1}{V}\int_{\mathcal{A}_{\gamma\sigma}}\mathbf{n}_{\gamma\sigma}\\ &\cdot\left[-\tilde{p}_\gamma\mathbf{I} + \mu_\gamma\nabla\tilde{\mathbf{v}}_\gamma\right]d\mathcal{A}.\end{aligned} \tag{29}$$

Combining LHS and RHS gives us the averaged equation:

$$\begin{aligned}&\rho_\gamma\frac{\partial\langle\mathbf{v}_\gamma\rangle^\gamma}{\partial t} + \rho_\gamma\langle\mathbf{v}_\gamma\rangle^\gamma\cdot\nabla\langle\mathbf{v}_\gamma\rangle^\gamma + \varepsilon_\gamma^{-1}\nabla\cdot(\rho_\gamma\langle\tilde{\mathbf{v}}_\gamma\tilde{\mathbf{v}}_\gamma\rangle)\\ &= -\nabla\langle p_\gamma\rangle^\gamma + \rho_\gamma\mathbf{g} + \nabla\cdot(\langle\mu_\gamma\rangle^\gamma\nabla\langle\mathbf{v}_\gamma\rangle^\gamma) + \varepsilon_\gamma^{-1}\nabla\cdot\langle\mu_\gamma\nabla\tilde{\mathbf{v}}_\gamma\rangle\\ &\quad + \varepsilon_\gamma^{-1}\langle\nabla\tilde{\mu}_\gamma\rangle\cdot\nabla\langle\mathbf{v}_\gamma\rangle^\gamma + \frac{\varepsilon_\gamma^{-1}}{V}\int_{\mathcal{A}_{\gamma\sigma}}\mathbf{n}_{\gamma\sigma}\cdot\left[-\tilde{p}_\gamma\mathbf{I} + \mu_\gamma\nabla\tilde{\mathbf{v}}_\gamma\right]d\mathcal{A}.\end{aligned} \tag{30}$$

We notice that, if we assume that $\tilde{\mu}_\gamma = 0$, then we recover the formulation proposed by Whitaker [52] in the case of inertial flow where the viscosity is constant.

At this stage of the development, the averaged momentum equations are not under a closed form since velocity and pressure deviations having microscopic length-scale are still present. The classical strategy is to derive a problem that governs the deviations, then to represent them in terms of average quantities (the so-called closure problem), and, finally, to insert these representations into the conservation equation (30) to get the closed form of the averaged equations.

4. Mathematical problem governing the deviations

The aim of this section is to develop the relationships between spatial deviations and average quantities in order to close the macroscopic model.

4.1. Continuity equation

We form the equation that governs the deviation continuity equation in the γ-phase by subtracting Eq. (20) from Eq. (9). We obtain,

$$\nabla\cdot\tilde{\mathbf{v}}_\gamma = 0 \ \texttt{in}\ V_\gamma. \tag{31}$$

4.2. Momentum equation

We can now follow an equivalent procedure for the momentum balance. Subtracting Eq. (30) from Eq. (21) and considering the decompositions yields in

$$\begin{aligned}&\rho_\gamma\frac{\partial\tilde{\mathbf{v}}_\gamma}{\partial t} + \rho_\gamma\left(\mathbf{v}_\gamma\cdot\nabla\mathbf{v}_\gamma - \langle\mathbf{v}_\gamma\rangle^\gamma\cdot\nabla\langle\mathbf{v}_\gamma\rangle^\gamma\right) - \varepsilon_\gamma^{-1}\nabla\cdot(\rho_\gamma\langle\tilde{\mathbf{v}}_\gamma\tilde{\mathbf{v}}_\gamma\rangle)\\ &= -\nabla\tilde{p}_\gamma + \nabla\cdot\left(\mu_\gamma\nabla\mathbf{v}_\gamma - \langle\mu_\gamma\rangle^\gamma\nabla\langle\mathbf{v}_\gamma\rangle^\gamma\right) - \varepsilon_\gamma^{-1}\nabla\cdot\langle\mu_\gamma\nabla\tilde{\mathbf{v}}_\gamma\rangle\\ &\quad - \varepsilon_\gamma^{-1}\langle\nabla\tilde{\mu}_\gamma\rangle\cdot\nabla\langle\mathbf{v}_\gamma\rangle^\gamma - \frac{\varepsilon_\gamma^{-1}}{V}\int_{\mathcal{A}_{\gamma\sigma}}\mathbf{n}_{\gamma\sigma}\cdot\left[-\tilde{p}_\gamma\mathbf{I} + \mu_\gamma\nabla\tilde{\mathbf{v}}_\gamma\right]d\mathcal{A}.\end{aligned} \tag{32}$$

Considering that

$$\mathbf{v}_\gamma\cdot\nabla\mathbf{v}_\gamma - \langle\mathbf{v}_\gamma\rangle^\gamma\cdot\nabla\langle\mathbf{v}_\gamma\rangle^\gamma = \mathbf{v}_\gamma\cdot\nabla\tilde{\mathbf{v}}_\gamma + \tilde{\mathbf{v}}_\gamma\cdot\nabla\langle\mathbf{v}_\gamma\rangle^\gamma \tag{33}$$

and that

$$\begin{aligned}\nabla\cdot\left(\mu_\gamma\nabla\mathbf{v}_\gamma - \langle\mu_\gamma\rangle^\gamma\nabla\langle\mathbf{v}_\gamma\rangle^\gamma\right) &= \nabla\cdot\left(\mu_\gamma\nabla\tilde{\mathbf{v}}_\gamma + \tilde{\mu}_\gamma\nabla\langle\mathbf{v}_\gamma\rangle^\gamma\right)\\ &= \nabla\cdot\left(\mu_\gamma\nabla\tilde{\mathbf{v}}_\gamma\right) + (\nabla\tilde{\mu}_\gamma)\cdot\nabla\langle\mathbf{v}_\gamma\rangle^\gamma + \tilde{\mu}_\gamma\nabla^2\langle\mathbf{v}_\gamma\rangle^\gamma,\end{aligned} \tag{34}$$

one can reformulate Eq. (33) as

$$\begin{aligned}&\rho_\gamma\frac{\partial\tilde{\mathbf{v}}_\gamma}{\partial t} + \rho_\gamma\mathbf{v}_\gamma\cdot\nabla\tilde{\mathbf{v}}_\gamma + \rho_\gamma\tilde{\mathbf{v}}_\gamma\cdot\nabla\langle\mathbf{v}_\gamma\rangle^\gamma - \varepsilon_\gamma^{-1}\nabla\cdot(\rho_\gamma\langle\tilde{\mathbf{v}}_\gamma\tilde{\mathbf{v}}_\gamma\rangle)\\ &= -\nabla\tilde{p}_\gamma + \nabla\cdot\left(\mu_\gamma\nabla\tilde{\mathbf{v}}_\gamma\right) + \left(\nabla\tilde{\mu}_\gamma - \langle\nabla\tilde{\mu}_\gamma\rangle^\gamma\right)\cdot\nabla\langle\mathbf{v}_\gamma\rangle^\gamma\\ &\quad + \tilde{\mu}_\gamma\nabla^2\langle\mathbf{v}_\gamma\rangle^\gamma - \varepsilon_\gamma^{-1}\nabla\cdot\langle\mu_\gamma\nabla\tilde{\mathbf{v}}_\gamma\rangle - \frac{\varepsilon_\gamma^{-1}}{V}\int_{\mathcal{A}_{\gamma\sigma}}\mathbf{n}_{\gamma\sigma}\cdot\left[-\tilde{p}_\gamma\mathbf{I} + \mu_\gamma\nabla\tilde{\mathbf{v}}_\gamma\right]d\mathcal{A}.\end{aligned} \tag{35}$$

We can realize some simplifications based on the assumption of length-scale separation. Indeed, if we note l_γ and L respectively the characteristic dimensions associated to microscopic and macroscopic spatial variations, we have the length-scale constraint

$$l_\gamma \ll L. \tag{36}$$

Under these circumstances, the convective and the dispersive terms that appear in the left hand side of Eq. (35) can be estimated by

$$\rho_\gamma\mathbf{v}_\gamma\cdot\nabla\tilde{\mathbf{v}}_\gamma = O\left(\rho_\gamma\frac{\max(\mathbf{v}_\gamma)^2}{l_\gamma}\right), \tag{37}$$

$$\rho_\gamma\tilde{\mathbf{v}}_\gamma\cdot\nabla\langle\mathbf{v}_\gamma\rangle^\gamma = O\left(\rho_\gamma\frac{\max(\mathbf{v}_\gamma)^2}{L}\right), \tag{38}$$

$$\varepsilon_\gamma^{-1}\nabla\cdot(\rho_\gamma\langle\tilde{\mathbf{v}}_\gamma\tilde{\mathbf{v}}_\gamma\rangle) = O\left(\rho_\gamma\frac{\max(\mathbf{v}_\gamma)^2}{L}\right). \tag{39}$$

Therefore, from the length-scale separation assumption equation (36) we deduce

$$\rho_\gamma\tilde{\mathbf{v}}_\gamma\cdot\nabla\langle\mathbf{v}_\gamma\rangle^\gamma \sim \varepsilon_\gamma^{-1}\nabla\cdot(\rho_\gamma\langle\tilde{\mathbf{v}}_\gamma\tilde{\mathbf{v}}_\gamma\rangle) \ll \rho_\gamma\mathbf{v}_\gamma\cdot\nabla\tilde{\mathbf{v}}_\gamma. \tag{40}$$

Moreover, according to Quintard and Whitaker [37], we can assume time scales separation as well, which leads us to neglect the accumulation term in Eq. (35).

The terms in the right hand side of Eq. (35) can be estimated by

$$\nabla\cdot\left(\mu_\gamma\nabla\tilde{\mathbf{v}}_\gamma\right)=O\left(\frac{\max(\mu_\gamma)\max(\mathbf{v}_\gamma)}{l_\gamma^2}\right), \tag{41}$$

$$\left(\nabla\tilde{\mu}_\gamma-\langle\nabla\tilde{\mu}_\gamma\rangle^\gamma\right)\cdot\nabla\langle\mathbf{v}_\gamma\rangle^\gamma=O\left(\frac{\max(\mu_\gamma)\max(\mathbf{v}_\gamma)}{l_\gamma L}\right), \tag{42}$$

$$\tilde{\mu}_\gamma\nabla^2\langle\mathbf{v}_\gamma\rangle^\gamma=O\left(\frac{\max(\mu_\gamma)\max(\mathbf{v}_\gamma)}{L^2}\right), \tag{43}$$

$$\varepsilon_\gamma^{-1}\nabla\cdot\langle\mu_\gamma\nabla\tilde{\mathbf{v}}_\gamma\rangle=O\left(\frac{\max(\mu_\gamma)\max(\mathbf{v}_\gamma)}{l_\gamma L}\right), \tag{44}$$

$$\frac{\varepsilon_\gamma^{-1}}{V}\int_{\mathcal{A}_{\gamma\sigma}}\mathbf{n}_{\gamma\sigma}\cdot\mu_\gamma\nabla\tilde{\mathbf{v}}_\gamma d\mathcal{A}=O\left(\frac{\max(\mu_\gamma)\max(\mathbf{v}_\gamma)}{l_\gamma^2}\right). \tag{45}$$

Then we deduce that

$$\begin{aligned}\tilde{\mu}_\gamma\nabla^2\langle\mathbf{v}_\gamma\rangle^\gamma &\ll\left(\nabla\tilde{\mu}_\gamma-\langle\nabla\tilde{\mu}_\gamma\rangle^\gamma\right)\cdot\nabla\langle\mathbf{v}_\gamma\rangle^\gamma\sim\varepsilon_\gamma^{-1}\nabla\cdot\langle\mu_\gamma\nabla\tilde{\mathbf{v}}_\gamma\rangle\\ &\ll\nabla\cdot\left(\mu_\gamma\nabla\tilde{\mathbf{v}}_\gamma\right)\sim\frac{\varepsilon_\gamma^{-1}}{V}\int_{\mathcal{A}_{\gamma\sigma}}\mathbf{n}_{\gamma\sigma}\cdot\mu_\gamma\nabla\tilde{\mathbf{v}}_\gamma d\mathcal{A}.\end{aligned} \tag{46}$$

Finally, after these simplifications, the closure equation for the momentum balance takes the form

$$\rho_\gamma\mathbf{v}_\gamma\cdot\nabla\tilde{\mathbf{v}}_\gamma=-\nabla\tilde{p}_\gamma+\nabla\cdot\left(\mu_\gamma\nabla\tilde{\mathbf{v}}_\gamma\right)-\frac{\varepsilon_\gamma^{-1}}{V}\int_{\mathcal{A}_{\gamma\sigma}}\mathbf{n}_{\gamma\sigma}\cdot\left[-\tilde{p}_\gamma\mathbf{I}+\mu_\gamma\nabla\tilde{\mathbf{v}}_\gamma\right]d\mathcal{A}. \tag{47}$$

It must be noticed that, in spite of the apparent similarity with the equation derived by Whitaker [52] in the case of laminar flow, the above equation deals with time-averaged quantities and *variable* viscosity.

4.3. Boundary conditions

The boundary condition associated with this deviation problem is obtained using $\mathbf{v}_\gamma=\langle\mathbf{v}_\gamma\rangle^\gamma+\tilde{\mathbf{v}}_\gamma$ into Eq. (11)

$$\tilde{\mathbf{v}}_\gamma=-\langle\mathbf{v}_\gamma\rangle^\gamma\ \texttt{at}\ \mathcal{A}_{\gamma\sigma}. \tag{48}$$

In addition, we have the condition equation (16) which says that average of the deviations must be zero

$$\langle\tilde{\mathbf{v}}_\gamma\rangle^\gamma=0;\quad\langle\tilde{p}_\gamma\rangle^\gamma=0. \tag{49}$$

In order to solve the closure problem in a representative region of the porous medium instead of considering the entire macro-structure, we consider the model of a spatially periodic system. Hence, we add the following periodic conditions to this deviation problem,

$$\tilde{\mathbf{v}}_\gamma(\mathbf{r}+\mathbf{l}_i)=\tilde{\mathbf{v}}_\gamma(\mathbf{r});\ \tilde{p}_\gamma(\mathbf{r}+\mathbf{l}_i)=\tilde{p}_\gamma(\mathbf{r});\quad i=1,2,3. \tag{50}$$

4.4. Deviation representations

Clearly $\langle\mathbf{v}_\gamma\rangle^\gamma$ appears as a non-homogeneous term in the boundary conditions for the closure problem, and this needs to be considered in the representation for the spatial deviations. We assume that the averaged velocity $\langle\mathbf{v}_\gamma\rangle^\gamma$ generates perturbations in each direction. The generated deviations can be very different with regards to the direction. Hence, to account for this potential anisotropy, we propose the following mapping:

$$\tilde{\mathbf{v}}_\gamma=\mathbf{B}_\gamma\cdot\langle\mathbf{v}_\gamma\rangle^\gamma;\quad\tilde{p}_\gamma=\mathbf{b}_\gamma\cdot\langle\mathbf{v}_\gamma\rangle^\gamma, \tag{51}$$

where $\mathbf{B}_\gamma$ is a tensor while $\mathbf{b}_\gamma$ is a vector. This representation differs slightly from the one usually proposed in the literature [51,52,50] since the viscosity is not included in the pressure representation. We could have, of course, introduced a reference viscosity in the second equation in Eq. (51) to recover the notations of the cited authors. However, that would not bring any interesting simplifications in the closure problem which is marked by the spatial variations of $\mu_\gamma(\mathbf{r})$, contrary to the cited literature. Authors use such a representation to obtain a permeability tensor that is independent from the fluid properties. However, in our study, the viscosity is space-dependent and consequently cannot be pulled out from integrals.

5. Closure problem

The next step of our development is to establish the mathematical problem that will allow us to determine the closure variables $\mathbf{B}_\gamma$ and $\mathbf{b}_\gamma$. This problem will be solved over a periodic representative unit-cell. It is obtained by substituting the above suggested mapping equation (51) into the deviations problem of Section 4. The identification of each term involving $\langle\mathbf{v}_\gamma\rangle^\gamma$ provides the following closure problem

$$\begin{aligned}\rho_\gamma\mathbf{v}_\gamma\cdot\nabla\mathbf{B}_\gamma=&-\nabla\mathbf{b}_\gamma+\nabla\cdot\left(\mu_\gamma\nabla\mathbf{B}_\gamma\right)\\ &-\frac{\varepsilon_\gamma^{-1}}{V}\int_{\mathcal{A}_{\gamma\sigma}}\mathbf{n}_{\gamma\sigma}\cdot\left[-\mathbf{b}_\gamma\mathbf{I}+\mu_\gamma\nabla\mathbf{B}_\gamma\right]d\mathcal{A}\ \texttt{in}\ V_\gamma,\end{aligned} \tag{52}$$

$$\nabla\cdot\mathbf{B}_\gamma=\mathbf{0}\ \texttt{in}\ V_\gamma, \tag{53}$$

$$\mathbf{B}_\gamma=-\mathbf{I}\ \texttt{at}\ \mathcal{A}_{\gamma\sigma}, \tag{54}$$

$$\mathbf{B}_\gamma(\mathbf{r}+\mathbf{l}_i)=\mathbf{B}_\gamma(\mathbf{r});\quad\mathbf{b}_\gamma(\mathbf{r}+\mathbf{l}_i)=\mathbf{b}_\gamma(\mathbf{r});\ i=1,2,3, \tag{55}$$

$$\langle\mathbf{B}_\gamma\rangle^\gamma=\mathbf{0};\quad\langle\mathbf{b}_\gamma\rangle^\gamma=\mathbf{0}. \tag{56}$$

At this point of the development, we derived an integro-differential boundary value problem. We recognize a Navier–Stokes-like problem that involves additionnal source terms.

The resolution of such a problem can be simplified using a special change of variables. This will allow to free oneself from the presence of integrals and other source terms within the governing equations. We propose the following change of variables:

$$\mathbf{B}_\gamma^0=(\mathbf{B}_\gamma+\mathbf{I})\cdot\mathbf{C}_\gamma^{-1};\quad\mathbf{b}_\gamma^0=\mathbf{b}_\gamma\cdot\mathbf{C}_\gamma^{-1}, \tag{57}$$

where we have defined $\mathbf{C}_\gamma$ as

$$\mathbf{C}_\gamma=\frac{\varepsilon_\gamma^{-1}}{V}\int_{\mathcal{A}_{\gamma\sigma}}\mathbf{n}_{\gamma\sigma}\cdot\left[-\mathbf{b}_\gamma\mathbf{I}+\mu_\gamma\nabla\mathbf{B}_\gamma\right]d\mathcal{A}. \tag{58}$$

Finally, we obtain the following closure problem

$$\rho_\gamma\mathbf{v}_\gamma\cdot\nabla\mathbf{B}_\gamma^0=-\nabla\mathbf{b}_\gamma^0+\nabla\cdot\left(\mu_\gamma\nabla\mathbf{B}_\gamma^0\right)-\mathbf{I}\ \texttt{in}\ V_\gamma, \tag{59}$$

$$\nabla\cdot\mathbf{B}_\gamma^0=\mathbf{0}\ \texttt{in}\ V_\gamma, \tag{60}$$

$$\mathbf{B}_\gamma^0=\mathbf{0}\ \texttt{at}\ \mathcal{A}_{\gamma\sigma}, \tag{61}$$

$$\mathbf{B}_\gamma^0(\mathbf{r}+\mathbf{l}_i)=\mathbf{B}_\gamma^0(\mathbf{r});\quad\mathbf{b}_\gamma^0(\mathbf{r}+\mathbf{l}_i)=\mathbf{b}_\gamma^0(\mathbf{r});\ i=1,2,3. \tag{62}$$

The tensor $\mathbf{C}_\gamma$ is a result of the simulation and can be evaluated through the average value of $\mathbf{B}_\gamma^0$. Moreover, to insure uniqueness of the solution, we must constrain the $\mathbf{b}_\gamma^0$ field, which gives:

$$\langle\mathbf{B}_\gamma^0\rangle^\gamma=\mathbf{C}_\gamma^{-1}\ ;\quad\langle\mathbf{b}_\gamma^0\rangle^\gamma=0. \tag{63}$$

6. Closed form of the averaged momentum equation

We form the macroscopic equation by introducing the representation of the deviation as a function of the average velocity, Eq. (51) within the non-closed averaged momentum equation, (30). However, before to carry out such an operation, we will

analyze the order of magnitude of each term in order to simplify this equation. We recall here the non-closed macroscopic equation,

$$\rho_\gamma \frac{\partial \langle \mathbf{v}_\gamma \rangle^\gamma}{\partial t} + \rho_\gamma \langle \mathbf{v}_\gamma \rangle^\gamma \cdot \nabla \langle \mathbf{v}_\gamma \rangle^\gamma + \varepsilon_\gamma^{-1} \nabla \cdot (\rho_\gamma \langle \tilde{\mathbf{v}}_\gamma \tilde{\mathbf{v}}_\gamma \rangle) = -\nabla \langle p_\gamma \rangle^\gamma + \rho_\gamma \mathbf{g} + \nabla \cdot (\langle \mu_\gamma \rangle^\gamma \nabla \langle \mathbf{v}_\gamma \rangle^\gamma) + \varepsilon_\gamma^{-1} \nabla \cdot \langle \mu_\gamma \nabla \tilde{\mathbf{v}}_\gamma \rangle + \varepsilon_\gamma^{-1} \langle \nabla \tilde{\mu}_\gamma \rangle \cdot \nabla \langle \mathbf{v}_\gamma \rangle^\gamma + \frac{\varepsilon_\gamma^{-1}}{V} \int_{\mathcal{A}_{\gamma\sigma}} \mathbf{n}_{\gamma\sigma} \cdot \left[-\tilde{p}_\gamma \mathbf{I} + \mu_\gamma \nabla \tilde{\mathbf{v}}_\gamma \right] d\mathcal{A}, \quad (64)$$

For the term in the right hand side of Eq. (64) we have the following estimations

$$\frac{\varepsilon_\gamma^{-1}}{V} \int_{\mathcal{A}_{\gamma\sigma}} \mathbf{n}_{\gamma\sigma} \cdot \mu_\gamma \nabla \tilde{\mathbf{v}}_\gamma d\mathcal{A} = O\left(\frac{\max(\mu_\gamma) \max(\mathbf{v}_\gamma)}{l_\gamma^2} \right), \quad (65)$$

$$\nabla \cdot (\langle \mu_\gamma \rangle^\gamma \nabla \langle \mathbf{v}_\gamma \rangle^\gamma) = O\left(\frac{\max(\mu_\gamma) \max(\mathbf{v}_\gamma)}{L^2} \right), \quad (66)$$

$$\varepsilon_\gamma^{-1} \nabla \cdot \langle \mu_\gamma \nabla \tilde{\mathbf{v}}_\gamma \rangle = O\left(\frac{\max(\mu_\gamma) \max(\mathbf{v}_\gamma)}{l_\gamma L} \right), \quad (67)$$

$$\varepsilon_\gamma^{-1} \langle \nabla \tilde{\mu}_\gamma \rangle \cdot \nabla \langle \mathbf{v}_\gamma \rangle^\gamma = O\left(\frac{\max(\mu_\gamma) \max(\mathbf{v}_\gamma)}{l_\gamma L} \right). \quad (68)$$

Consequently, based on the length-scale separation assumption equation (36) and the estimation equation (45) we deduce that

$$\nabla \cdot (\langle \mu_\gamma \rangle^\gamma \nabla \langle \mathbf{v}_\gamma \rangle^\gamma) \ll \varepsilon_\gamma^{-1} \nabla \cdot \langle \mu_\gamma \nabla \tilde{\mathbf{v}}_\gamma \rangle \sim \varepsilon_\gamma^{-1} \langle \nabla \tilde{\mu}_\gamma \rangle \cdot \nabla \langle \mathbf{v}_\gamma \rangle^\gamma \ll \frac{\varepsilon_\gamma^{-1}}{V} \int_{\mathcal{A}_{\gamma\sigma}} \mathbf{n}_{\gamma\sigma} \cdot \mu_\gamma \nabla \tilde{\mathbf{v}}_\gamma d\mathcal{A}. \quad (69)$$

We now focus on the evaluation of the order of magnitude of the term in the left hand side of Eq. (64) in front of the integral equation (65)

$$\rho_\gamma \langle \mathbf{v}_\gamma \rangle^\gamma \cdot \nabla \langle \mathbf{v}_\gamma \rangle^\gamma \Big/ \frac{\varepsilon_\gamma^{-1}}{V} \int_{\mathcal{A}_{\gamma\sigma}} \mathbf{n}_{\gamma\sigma} \cdot \mu_\gamma \nabla \tilde{\mathbf{v}}_\gamma d\mathcal{A} = O\left(\rho_\gamma \frac{\max(\mathbf{v}_\gamma)^2}{L} \frac{l_\gamma^2}{\max(\mu_\gamma) \max(\mathbf{v}_\gamma)} \right) = O\left(Re_{\gamma_{turb}} \frac{l_\gamma}{L} \right), \quad (70)$$

$$\varepsilon_\gamma^{-1} \nabla \cdot (\rho_\gamma \langle \tilde{\mathbf{v}}_\gamma \tilde{\mathbf{v}}_\gamma \rangle) \Big/ \frac{\varepsilon_\gamma^{-1}}{V} \int_{\mathcal{A}_{\gamma\sigma}} \mathbf{n}_{\gamma\sigma} \cdot \mu_\gamma \nabla \tilde{\mathbf{v}}_\gamma d\mathcal{A} = O\left(\rho_\gamma \frac{\max(\mathbf{v}_\gamma)^2}{L} \frac{l_\gamma^2}{\max(\mu_\gamma) \max(\mathbf{v}_\gamma)} \right) = O\left(Re_{\gamma_{turb}} \frac{l_\gamma}{L} \right). \quad (71)$$

Clearly, these terms can be neglected if the Reynolds number is small enough. In other words, it means that the constraint,

$$Re_{\gamma_{turb}} = \frac{\rho_\gamma \max(\mathbf{v}_\gamma) l_\gamma}{\max(\mu_\gamma)} \ll \frac{L}{l_\gamma}, \quad (72)$$

must be satisfied, which is often true if the length scales are separated enough. From similar arguments, we can also neglect the accumulation term. All these simplifications give,

$$0 = -\nabla \langle p_\gamma \rangle^\gamma + \rho_\gamma \mathbf{g} + \left(\frac{\varepsilon_\gamma^{-1}}{V} \int_{\mathcal{A}_{\gamma\sigma}} \mathbf{n}_{\gamma\sigma} \cdot \left[-\mathbf{b}_\gamma \mathbf{I} + \mu_\gamma \nabla \mathbf{B}_\gamma \right] d\mathcal{A} \right) \cdot \langle \mathbf{v}_\gamma \rangle^\gamma. \quad (73)$$

Identifying the integral as $\mathbf{C}_\gamma$ it becomes,

$$0 = -\nabla \langle p_\gamma \rangle^\gamma + \rho_\gamma \mathbf{g} + \varepsilon_\gamma^{-1} \mathbf{C}_\gamma \cdot \langle \mathbf{v}_\gamma \rangle. \quad (74)$$

We can decompose the tensor $\mathbf{C}_\gamma$ into two parts. The first one will produce the Darcy's law permeability tensor that depends only on the geometry of the porous medium under consideration, the second part will lead to an inertial/turbulent correction:

$$\varepsilon_\gamma^{-1} \mathbf{C}_\gamma = -\mu_{\gamma_{mol}} \mathbf{K}^{-1} \cdot (\mathbf{I} + \mathbf{F}). \quad (75)$$

This way, we obtain a similar form of Darcy–Forchheimer equation derived by Whitaker [52]. However, in our case, $\mathbf{F}$ not only accounts for inertial effects but for turbulence effects as well via the viscosity spatial variations.

$$\langle \mathbf{v}_\gamma \rangle = -\frac{\mathbf{K}}{\mu_{\gamma_{mol}}} \cdot \left(\nabla \langle p_\gamma \rangle^\gamma - \rho_\gamma \mathbf{g} \right) - \mathbf{F} \cdot \langle \mathbf{v}_\gamma \rangle. \quad (76)$$

In this equation,

- one must keep in mind that $\langle \mathbf{v}_\gamma \rangle$ depicts the volume average of a local time-averaged velocity field and that $\langle p_\gamma \rangle^\gamma$ is the volume average of a local time-averaged local field described as a turbulent pressure,
- $\mathbf{K}$ is the permeability tensor and has the dimension of m^2. It is intrinsic to the porous medium pore-scale geometry. It is symmetric and positive definite [14]. It can be evaluated using the closure problem equations (59)–(63) when $\mathbf{v}_\gamma = 0$ and $\mu_\gamma(\mathbf{r}) = \mu_{\gamma_{mol}}$,
- $\mathbf{F}$ is the Forchheimer correction tensor (dimensionless) that account for both inertial and turbulence effect at macro-scale. In order to learn something about $\mathbf{F}$, one first needs to estimate $\mathbf{K}$ as pointed out by Whitaker [52], and then solve the closure problem equations (59)–(63) where $\mathbf{v}_\gamma$ and $\mu_\gamma(\mathbf{r})$ come from a preliminary turbulent microscopic simulations. Finally, $\mathbf{F}$ is merely deduced from Eq. (75). Note that $\mathbf{F}$ may strongly depend on these input fields and is not necessarily proportional to the velocity, as in the classical Forchheimer equation. Therefore, it must be tabulated based on several microscopic simulations. There is not, in general, a simple relationship allowing to extrapolate $\mathbf{F}$ between two different velocity field realizations. Therefore, tabulation must account for velocity magnitude and its orientation. At the opposite of what is generally believed, Lasseux et al. [20] proved that $\mathbf{F}$ is not always symmetric.

We can also directly evaluate an apparent permeability tensor $\mathbf{K}^*$ [13] defined as

$$\varepsilon_\gamma^{-1} \mathbf{C}_\gamma = -\mu_{\gamma_{mol}} \mathbf{K}^{*-1}, \quad (77)$$

i.e. $\mathbf{K}^{*-1} = \mathbf{K}^{-1} \cdot (\mathbf{I} + \mathbf{F})$. From this definition, one can easily note that $\mathbf{K}^*$ varies continuously with regards to the Reynolds number. This point is consistent with the experimental studies by Chauveteau and Thirriot [9]. Moreover, all the remarks concerning $\mathbf{F}$ are also available for $\mathbf{K}^*$. With such a definition, the macro-scale momentum equation becomes,

$$\langle \mathbf{v}_\gamma \rangle = -\frac{\mathbf{K}^*}{\mu_{\gamma_{mol}}} \cdot \left(\nabla \langle p_\gamma \rangle^\gamma - \rho_\gamma \mathbf{g} \right). \quad (78)$$

While the use of $\mu_{\gamma_{mol}}$ is consistent with the non-inertial limit, we should note that, at this point, we could have chosen another reference viscosity and that this would have changed the definition of $\mathbf{K}^*$.

We insist on the fact that to a microscopic velocity and a microscopic viscosity fields correspond a particular apparent permeability tensor $\mathbf{K}^*$. Therefore, all the tensor components depend on these local fields. They are consequently functions of the velocity *magnitude* and *orientation* and must be tabulated with regards to these two parameters.

7. Validation of the approach

We present in this section two-dimensional simulations with the objective to validate the mathematical up-scaling procedure

developed in this paper. Reference 3D simulations will be introduced in the next section.

7.1. Principle of the validation

To validate an up-scaling methodology, a common method consists in a comparison between the pore-scale numerical simulations of the flow over a geometry made of several representative unit-cells and the results from the macro-scale model. In such method, the pore-scale fields are averaged over unit-cells to form reference macro-scale fields. Because of the pore-scale computing cost, this method is often restricted to simple unit cell geometry like stratified media or arrays of beads. In this section, we propose to use another methodology to validate the upscaling process. It focuses upon the estimation of the pressure drop per unit-length itself $(\frac{\Delta P}{L})$ as will be described later. This pressure drop can be estimated from two different manners. The first one directly results from the simulation of the Reynolds Average Navier–Stokes equations over a Representative Elementary Volume. Due to the periodic feature of the REV, this pressure loss per unit-length also corresponds to the pressure drop through the whole domain. We will call it *"direct pressure drop"*. The second one derives from the application of the generalized Darcy–Forchheimer's law Eq. (78) resulting from the up-scaling analysis. In this case, we will talk about *"reconstructed pressure drop"*. This validation method itself suggests that the closure problem equations (59)–(63) is somehow an interpretation of the RANS simulation results. From a practical point of view, simulations performed to validate the proposed method are realized in two steps:

1. First, we carry out what we call a direct simulation over the REV in order to obtain the local velocity and viscosity fields. We impose a macroscopic pressure drop per unit length by adding a vector source term $(\frac{\Delta P}{L})_{direct}\mathbf{e}_0$ into the momentum equation of the turbulence model. The vector $\mathbf{e}_0$ determines the local fields orientation. Direct simulations are performed using the finite volume CFD toolbox OpenFOAM®. Gas flow is assumed to be steady-state within the REV. Therefore, we use the SIMPLE pressure–velocity coupling procedure proposed by Patankar [31] to solve the RANS problem. We adapt the existing *simpleFoam* solver to integrate the pressure drop source term in the momentum equation. The resulting velocity field is then volume averaged to obtain $\langle \mathbf{v}_\gamma \rangle_{direct}$.
2. In a second stage, the closure problem, as defined by Eqs. (59)–(63), is solved from the previous velocity and viscosity fields to evaluate $\mathbf{K}^*$. As for the first step, we program the equations in the framework of the OpenFOAM® platform using a SIMPLE procedure. The inputs are the velocity and turbulent viscosity fields computed at the first step. The output consists in the apparent permeability tensor $\mathbf{K}^*$ for the given micro-scale velocity field.

Finally, to validate the results, we compare the direct pressure drop of step (1) (i.e., $(\frac{\Delta P}{L})_{direct}\mathbf{e}_0$) with regards to the pressure drop reconstructed from Eq. (78). Hence, the relation

$$\left(\frac{\Delta P}{L}\right)_{direct}\mathbf{e}_0 = \left(\frac{\Delta P}{L}\right)_{reconstructed}\mathbf{e}_0 = -\mu_{\gamma_{mol}}\left(\mathbf{K}^{*-1}\cdot\langle\mathbf{v}_\gamma\rangle_{direct}\right) \tag{79}$$

must be satisfied. The principle of the validation is sketched in Fig. 2.

7.2. Turbulent flow through a straight tube

The first validation test consists in the up-scaling of a turbulent flow through a straight tube. In 2D, the tube is assimilated to a rectangle 1 cm thick. For this simple geometry, we define the REV as the vertical cross-sections. Although the apparent permeability is well-known and can be easily calculated in the range of inertial flows, it is not possible to obtain analytical calculations when turbulence is present. Consequently, even for as simple geometries as straight tubes, numerical simulations are necessary to account for turbulence effects. The turbulent flow is statistically steady and oriented along the x-axis.

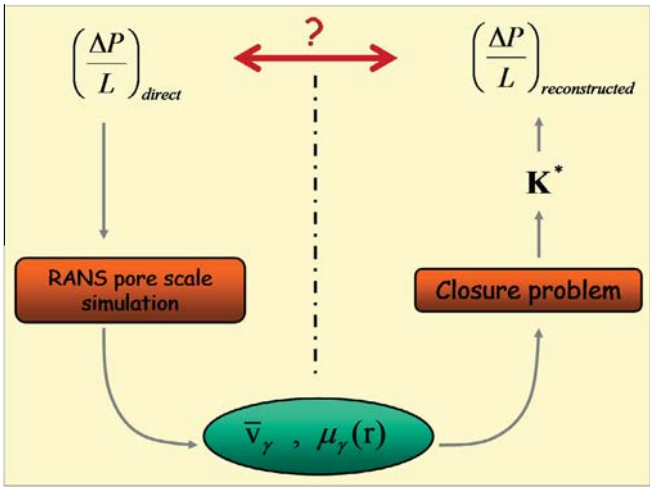

Fig. 2. Principle of the validation methodology. In one hand, the local fields are computed from numerical simulations with a pressure drop as source term. In another hand, the apparent permeability tensor is obtained from the calculation of the closure problem, and the pressure drop is then reconstructed using Darcy–Forchheimer law. Both pressure loss values should match to validate the upscaling.

We use the "Standard" $k-\epsilon$ model as described in Section 2 to obtain the microscopic fields. The flow behavior in the near wall region is approximated using the standard wall functions [54]. We use the following fluid properties, $\rho_\gamma = 1\ \mathrm{kg/m^3}, \mu_{\gamma_{mol}} = 10^{-5}\ \mathrm{kg/m/s}$ and we carry out calculations for pressure drops in the range $[14; 70\ \mathrm{Pa/m}]$, which corresponds to Reynolds numbers between 2600 and 7000.

Then, in a second time, the calculation of the closure problem, Eqs. (59)–(63), provides the apparent permeability tensor. As expected from the geometry shape, only the diagonal coefficients are non-zero. Hence, we can reconstruct the pressure drop with

$$\left(\frac{\Delta P}{L}\right)_{reconstructed} = -\mu_{\gamma_{mol}}\frac{\langle v_{\gamma_x}\rangle_{direct}}{K^*_{xx}}. \tag{80}$$

The comparison between both results is shown in Fig. 3. We can observe that the "direct" and "reconstructed" pressure drops are in fairly good agreement, which is an argument toward the validation of the macro-scale model proposed in this paper, as well as the upscaling procedure.

7.3. Turbulent flow through a simple array of beads

In this section we analyze the upscaling of turbulent flows through a two-dimensional array of beads. The equations for the microscopic flow and the closure problem are numerically solved inside the REV depicted in Fig. 4. With such a geometry, the porosity is $\varepsilon_\gamma \approx 0.8$. Periodic boundary conditions are defined on vertical edges and wall conditions are defined on both horizontal edges and bead outline as depicted in Fig. 4. As previously, simulations of the fully turbulent flow regime are performed using the $k-\epsilon$ method and the standard wall functions. Calculations are carried out for Reynolds number from 10^4 up to $5\cdot 10^4$.

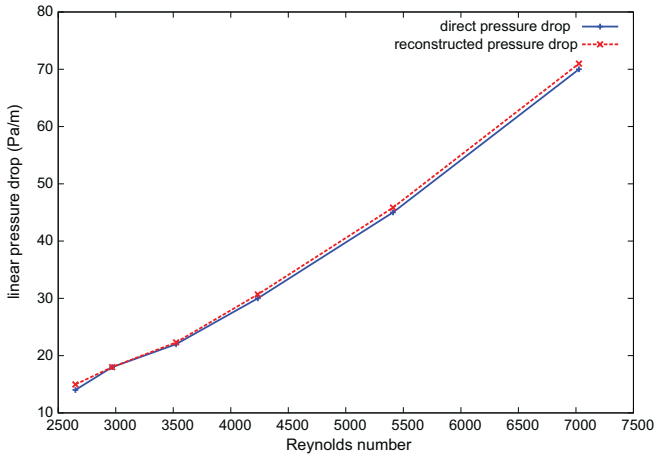

Fig. 3. Comparison of the pressure drops, $\frac{\Delta P}{L}$, evaluated through the direct and the reconstructed methodologies for the case of the tube. Both results are in good agreement.

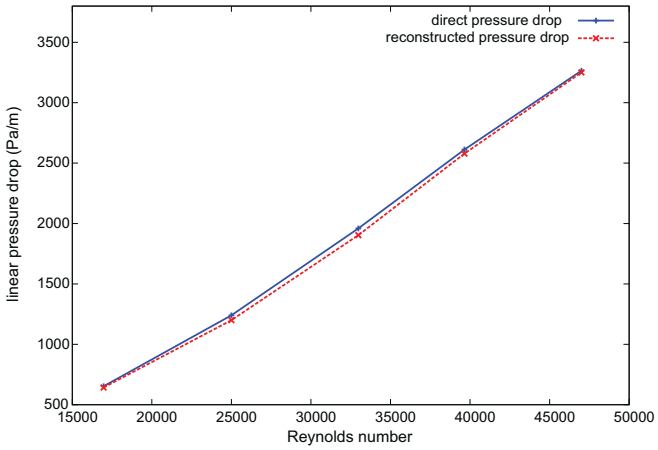

Fig. 5. Comparison of the pressure drops, $\frac{\Delta P}{L}$, evaluated through the direct and the reconstructed methodologies for the case of a simple array of beads. Both results are in good agreement.

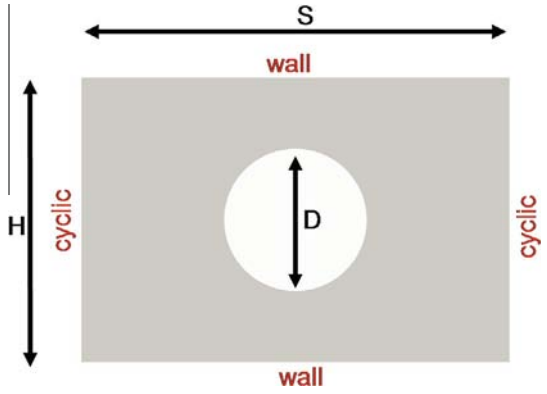

Fig. 4. Figure of the Representative Elementary Volume used to simulate flow in a simple array of beads. In this geometry, $D = 5$ mm,$H = 10$ mm and $S = 15$ mm. The grid is made of 10,000 cells.

The apparent permeability tensor is then evaluated from the resolution of the closure problem, Eqs. (59)–(63). As expected from the geometry shape, the non-diagonal coefficients are zero and the pressure drop can be reconstructed using Eq. (80). Both *direct* and *reconstructed* pressure drops are shown in Fig. 5. As in the previous example, they are in good agreement, so we can consider that the methodology developed hereby to interpret turbulent local fields in term of a generalized Darcy–Forchheimer law is validated. In the next section, simulations will provide additional validations for 3D geometries characteristic of structured packings.

8. Application to structured packings

In this section, we apply our methodology to structured packings used in chemical engineering reactors. These devices are made up of an assembly of corrugated sheets where two adjacent sheets are respectively inclined by an angle and the opposite of this angle from the vertical axis denoted by y in all this section (see Fig. 6). In our example, this angle is equal to 45°. The crossing junction of two "channels" forms the Representative Elementary Volume as depicted in Fig. 6. This pattern is repeated million times within the packing. The flow through this microscopic pattern leads to anisotropic flows at larger scales and this anisotropy must be characterized to design enhanced materials.

According to the present theory, the macro-scale momentum equation can be modeled by a generalized Darcy–Forchheimer law where the superficial velocity is related to the pressure gradient through an apparent permeability tensor $\mathbf{K}^*$. This tensor involves 9 components that depend on both the orientation and the magnitude of the velocity field. This representation, complex in appearance, can be simplified as described below. Indeed, although the microscopic flow field confined between two adjacent corrugated sheets is three dimensional, as depicted in Fig. 7, the macroscopic flow is essentially 2D. Therefore, the macro-scale momentum equation, for one packing element oriented in the x-direction, reads neglecting gravity effects

$$\langle \mathbf{v}_\gamma \rangle = -\frac{1}{\mu_{\gamma_{mol}}} \begin{pmatrix} K^*_{xx} & K^*_{xy} & 0 \\ K^*_{yx} & K^*_{yy} & 0 \\ 0 & 0 & 0 \end{pmatrix} \cdot \nabla \langle p_\gamma \rangle^\gamma, \tag{81}$$

where y denotes the vertical axis.

Usually, distillation columns are filled with several layers of structured packings which are alternatively rotated around the column axis by 90°relative to each other in order to improve liquid distribution. Consequently, the next packing is oriented in the z direction and the macroscale momentum equation becomes:

$$\langle \mathbf{v}_\gamma \rangle = -\frac{1}{\mu_{\gamma_{mol}}} \begin{pmatrix} 0 & 0 & 0 \\ 0 & K^*_{yy} & K^*_{yz} \\ 0 & K^*_{zy} & K^*_{zz} \end{pmatrix} \cdot \nabla \langle p_\gamma \rangle^\gamma. \tag{82}$$

Due to the packings rotation, K^*_{xx} and K^*_{zz} must obey the same law. Same arguments yield in $K^*_{xy} = K^*_{zy}$ and $K^*_{yx} = K^*_{yz}$. Therefore, the evaluation of the apparent permeability tensor in one packing is necessary to simulate the flow through industrial columns made of several packings. Mahr and Mewes [22] and Raynal and Royon-Lebeaud [43] state that the non-diagonal terms are negligible. Moreover, Raynal and Royon-Lebeaud [43] assumes that since the geometry of the REV does not vary if it is seen with regards to the x- or the y-axis, then the diagonal coefficients must be equal. To analyze these statements, we perform simulations in a large range of mass flow rate to scan the different macro-scale flow regimes, from the creeping flow regime to the fully turbulent flow regime:

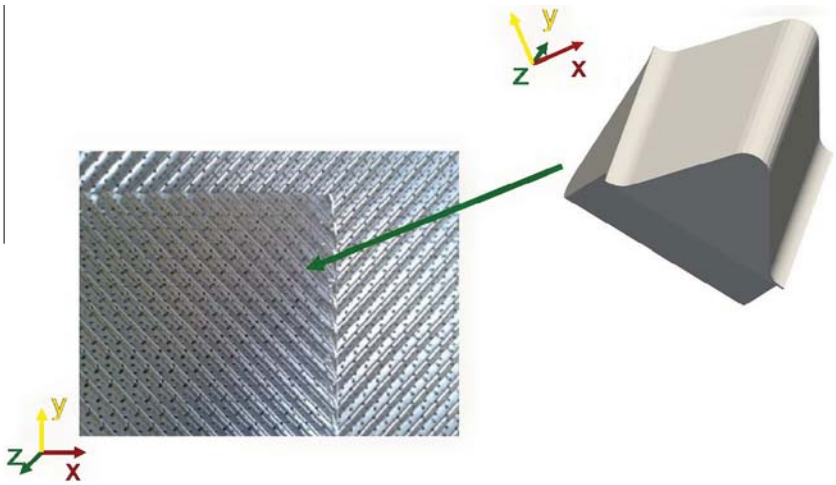

Fig. 6. (a) Picture of a structured packing made of an assembly of corrugated sheets where two adjacent sheets are respectively inclined by an angle and the opposite of this angle from the vertical axis. In the case under study, this angle is equal to 45°. (b) The Representative Elementary Volume made of the crossing junction of two adjacent corrugated sheets. The grid is made of more than 700,000 cells to ensure good results in turbulence flow regime.

- We start with the creeping flow regime. From a macro-scale point of view, it corresponds to the Darcy's regime, i.e., the pressure drop is strictly proportional to the superficial average velocity,
- Then, laminar simulations are performed up to the apparition of turbulence effects.
- Finally, the turbulent flow is simulated with the $k\Omega$-SST method.

To insure good results, especially in the investigation of the turbulent flow regime, we had to use a very fine grid made of more than 700,000 hexahedral cells. For the simulations we have used the following set of fluid properties: $\rho_\gamma = 4\ \mathrm{kg/m^3}, \mu_{\gamma_{mol}} = 5\ \mathrm{kg/m/s}$.

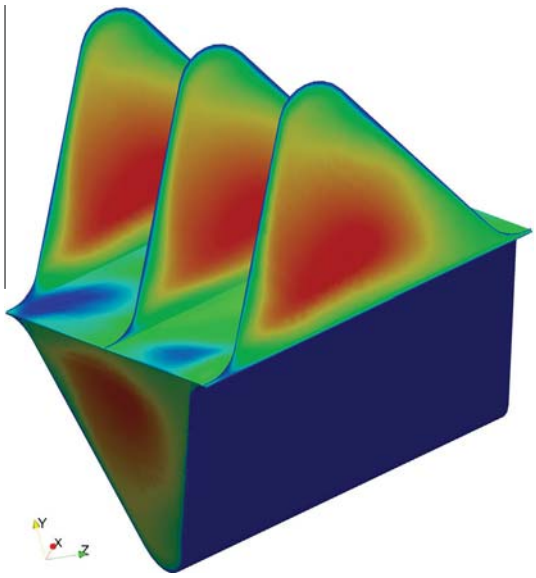

Fig. 7. Plot of the local magnitude velocity field in the REV. Although the microscopic field is 3D, the corresponding macro-scale velocity profile is essentially 2D. To investigate turbulence effects, the grid is made of more than 700,000 hexahedral cells.

8.1. Calculation of the intrinsic permeability

We first evaluate the permeability tensor by solving the boundary value problem equations (59)–(63) with $\mathbf{v}_\gamma = 0$ and $\mu_\gamma(\mathbf{r}) = \mu_{\gamma_{mol}}$. From the symmetry of the REV, we clearly deduce that the non-diagonal coefficients are zeros. This point is validated by the simulations. Moreover, since the shape of the REV is invariant if one examines it with regards to the x- or the y-axis, it was also expected to find that $K_{xx} = K_{yy}$. We obtain $K_{xx} = K_{yy} = K_0 = 610^{-7} m^2$. Hence, for this particular packing, the permeability tensor $\mathbf{K}$ is isotropic in the 2D plan xOy and we have:

$$\mathbf{K} = \begin{pmatrix} K_0 & 0 & 0 \\ 0 & K_0 & 0 \\ 0 & 0 & 0 \end{pmatrix}. \tag{83}$$

8.2. Laminar simulations

Then, we perform laminar simulations to investigate the form of the apparent permeability tensor $\mathbf{K}^*$ in inertial flow regimes. In normal functioning service, the gas flows through the distillation columns along the vertical axis. We study this configuration by imposing a macroscopic pressure drop in the vertical axis ($\mathbf{e}_0 = \mathbf{e}_y$) with $(\frac{\Delta P}{L})_{direct}$ varying in the range $[0.01,\ 2\ \mathrm{Pa/m}]$ which corresponds to Reynolds numbers in the range $[5,\ 550]$. The apparent permeability tensor is evaluated by solving the boundary value problem equations (59)–(63) with $\mu_\gamma(\mathbf{r}) = \mu_{\gamma_{mol}}$ and $\mathbf{v}_\gamma$ obtained from the flow simulations in the REV. It appears that there is a several orders of magnitude difference between the diagonal and the other terms. So, these latter terms can be neglected and the *reconstructed pressure drop* is evaluated using

$$\left(\frac{\Delta P}{L}\right)_{reconstructed} = -\mu_{\gamma_{mol}} \frac{\langle v_{\gamma_y} \rangle_{direct}}{K^*_{yy}}. \tag{84}$$

Following the methodology introduced in Section 7 we compare the *direct* and the *reconstructed pressure drops*. From their representations in Fig. 8 we can observe that they are in very good agreement. This point validate the current approach for laminar flows in a three-dimensional geometry.

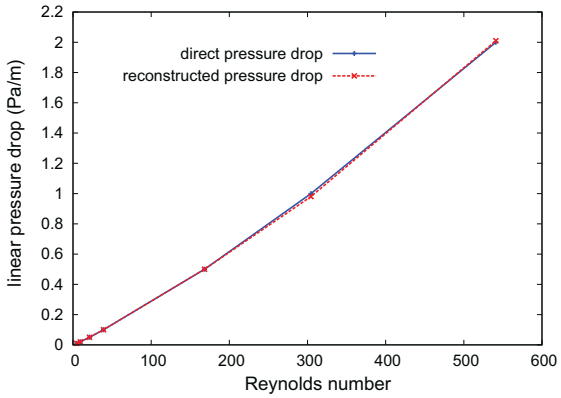

Fig. 8. Plot of the *direct* and *reconstructed pressure drops* in laminar flow regime. Both results are in good agreement which is a validation point of the present theory.

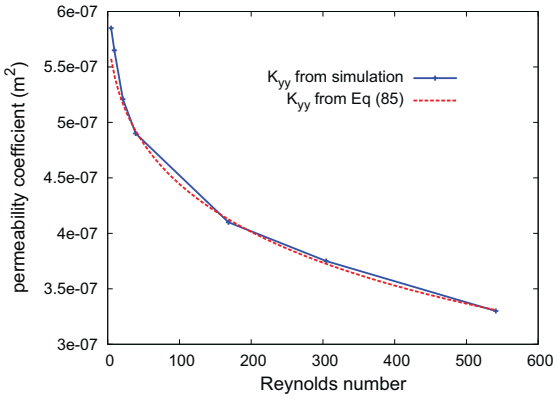

Fig. 9. Plot of the apparent permeability value in the vertical direction with regards to the mass flow rate in laminar regime. Results may be correlated by $K^*_{yy} = \frac{K_0}{1+\gamma_l\sqrt{Re}}$.

The resulting apparent permeability coefficient in the streamwise direction is plotted in Fig. 9 for different mass flow rates. We notice that the permeability coefficient in the main flow direction can be correlated by

$$K^*_{yy} = \frac{K_0}{1+\gamma_l\sqrt{Re}}, \tag{85}$$

where K_0 is the permeability and γ_l is a dimensionless fitting coefficient. It has been estimated equal to $\gamma_l = 0.035$. This correlation is reminiscent of Chauveteau and Thirriot [8] proposal in the case of fully developed inertia terms. It is also in agreement with the work by Skjetne and Auriault [46] who derived a similar law from the homogenization of the laminar, incompressible steady flow problem also in the case of fully developed inertia but with no turbulence. We may also note that the correlation proposed by Stichlmair et al. [49] to predict dry pressure drops in structured packings involves a correction term in $\sqrt{Re}$, as well.

In case of malfunction of the distillation process like the flooding of pores by the liquid phase, the orientation of the velocity fields in the neighborhood of the flooding area may be highly impacted. In such cases, the local velocity field is deflected from the vertical axis. In order to study the flow orientation-dependency of the permeability tensor $\mathbf{K}^*$, we have made several simulations imposing a macroscopic pressure drop with $\left(\frac{\Delta P}{L}\right)_{direct} = 0.5\ Pa/m$ (which corresponds to $Re \approx 170$) and a flow orientation

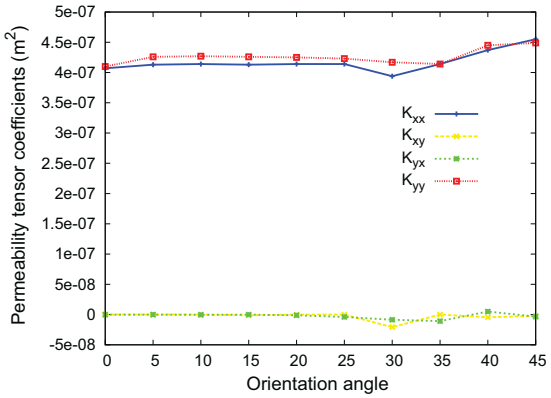

Fig. 10. Plot of the permeability coefficients value with respect to the flow orientation. The simulations correspond to $Re \approx 170$. We note that (i) the non-diagonal coefficients are negligible, (ii) the permeability coefficients do not strongly vary with the orientation angle, and (iii) we approximately have $K^*_{xx} \approx K^*_{yy}$.

$\mathbf{e}_0 = \begin{pmatrix} \cos\theta \\ \sin\theta \\ 0 \end{pmatrix}$ with θ varying in the range $[0, \frac{\Pi}{4}]$. We plot in Fig. 10 the values of the permeability coefficients $K^*_{xx}, K^*_{xy}, K^*_{yx}$ and K^*_{yy} with respect to the flow orientation angle. These results suggest the following remarks: (i) the non-diagonal coefficients are clearly negligible in comparison with the diagonal terms, (ii) the value of the permeability coefficients is almost constant and we can conclude that the flow orientation has no impact on the value of $\mathbf{K}^*$ for this particular structure, (iii) finally, we notice that the diagonal terms are almost equal ($K^*_{xx} \approx K^*_{yy}$). Although the initial problem seems quite complex (9 coefficients that depend on the flow magnitude and the flow orientation), it can be simplified and the apparent permeability tensor $\mathbf{K}^*$ may be described by the following simple expressions

$$\mathbf{K}^*(Re,\theta) \approx \begin{pmatrix} \frac{K_0}{1+\gamma_l\sqrt{Re}} & 0 & 0 \\ 0 & \frac{K_0}{1+\gamma_l\sqrt{Re}} & 0 \\ 0 & 0 & 0 \end{pmatrix}. \tag{86}$$

These conclusions however are restricted to the particular case of packings where the corrugated sheet are inclined by 45°from the column axis. One should perform the overall investigation again to characterize the macro-scale properties for other devices.

8.3. Turbulent simulations

To perform simulations in the turbulent regime, we choose the $k\Omega$-SST model which was found to give good results in the literature to simulate turbulent flows in structured packings [29,45,41,18]. In these simulations, the near wall regions are treated following the blending approach by Menter and Esch [25]. The apparent permeability tensor is evaluated by solving the boundary value problem equations (59)–(63) with $\mu_\gamma(\mathbf{r})$ and $\mathbf{v}_\gamma$ obtained from the turbulent flow simulations in the REV. As previously, to determine the full apparent permeability tensor $\mathbf{K}^*$ in the turbulent flow regime, we investigate the influence of the local fields with regards to, (i) the flow magnitude, and (ii) the flow orientation.

To study the first point, we perform flow simulations by imposing a macroscopic pressure drop in the vertical axis ($\mathbf{e}_0 = \mathbf{e}_y$) with $\left(\frac{\Delta P}{L}\right)_{direct}$ varying in the range [35, 120 Pa/m], which corresponds to Reynolds numbers in the range [3500, 5000]. As for the laminar case, it appears that differences of several orders of magnitude exist between the diagonal and the other terms. So, these latter terms

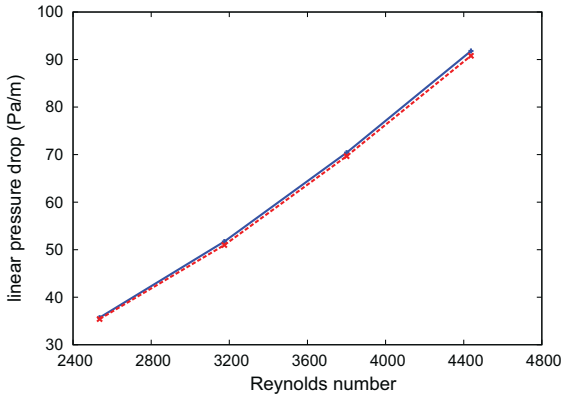

Fig. 11. Plot of the *direct* and *reconstructed pressure drops* in turbulent flow regime. Both results are in good agreement which is a validation point of the present theory.

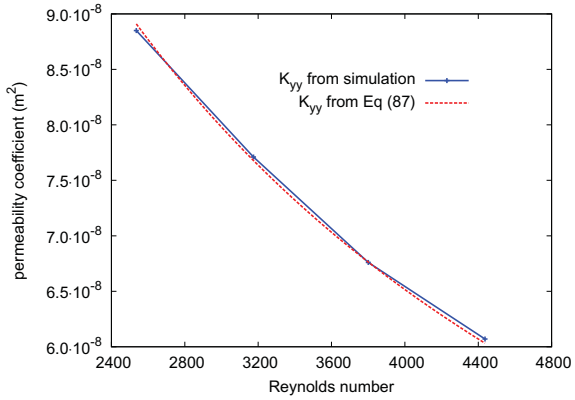

Fig. 12. Plot of the apparent permeability value in the vertical direction with regards to the mass flow rate in turbulent regime. Results may be correlated by $K^*_{yy} = \frac{K_1}{1+\gamma_t Re}$.

can be neglected and the *reconstructed pressure drop* is evaluated using Eq. (84). We plot in Fig. 11 the *direct* and *reconstructed pressure drops* we got from these simulations. Both are in very good agreement, which is an additional validation point for the theory introduced in the present paper. The resulting apparent permeability coefficient in the vertical direction is plotted in Fig. 12 as a function of the Reynolds number. We note that it can be correlated by

$$K^*_{yy} = \frac{K_1}{1+\gamma_t Re}, \tag{87}$$

where γ_t is a dimensionless fitting coefficient, and K_1 has the dimension of permeability (m^2) but, as pointed out by Skjetne and Auriault [46], it does not necessary refer to the intrinsic permeability value. They have been estimated equal to $\gamma_l = 6.9\,10^{-4}$ and $K_1 = 2.35\,10^{-7}\,\mathrm{m}^2$. This formulation is reminiscent of Ergun [15] work as well as most of the empirical structured packing dry pressure drop correlations [4,3,44].

In a second step, we investigate the value of the apparent permeability tensor with regards to the local velocity field orientation by imposing a macroscopic pressure drop with $\left(\frac{\Delta P}{L}\right)_{direct} = 90\,\mathrm{Pa/m}$ (which correspond to $Re \approx 4300$) and a flow orientation $\mathbf{e}_0 = \begin{pmatrix} \cos\theta \\ \sin\theta \\ 0 \end{pmatrix}$ with θ varying in the range $[0, \frac{\Pi}{4}]$. Once again, we can observe in Fig. 13 that, (i) the non-diagonal coefficients are negligible, (ii) the permeability coefficients do not strongly vary

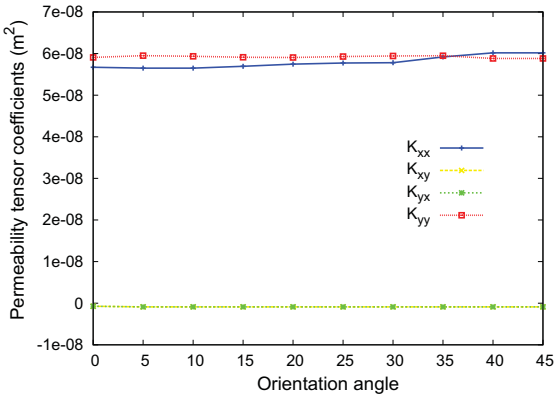

Fig. 13. Plot of the permeability coefficients value with regards to the flow orientation. The simulations correspond to $Re \approx 4300$. We note that (i) the non-diagonal coefficients are negligible, (ii) the permeability coefficients do not strongly vary with regards to the orientation angle, and (iii) we approximatively have $K^*_{xx} \approx K^*_{yy}$.

with regards to the orientation angle, and (iii) we approximatively have $K^*_{xx} \approx K^*_{yy}$.

Finally, to model high flow rate in structured packing, we can use the following permeability tensor:

$$\mathbf{K}^*(Re,\theta) \approx \begin{pmatrix} \frac{K_1}{1+\beta_t Re} & 0 & 0 \\ 0 & \frac{K_1}{1+\beta_t Re} & 0 \\ 0 & 0 & 0 \end{pmatrix}. \tag{88}$$

As it was indicated in the laminar case, this relation is restricted to the particular case of structured packings with corrugated sheets rotated by 45°with regards to the vertical axis and conclusion may be different in other configurations.

9. Conclusions and perspectives

At this point, we have developed a macro-scale model with closure for an incompressible single phase flow in a porous medium in the presence of turbulence. The momentum and continuity equations of a general RANS model have been volume averaged, assuming that all the turbulent information is included in a variable viscosity. The resulting macro-scale momentum balance equation has the form of a generalized Darcy–Forchheimer law with tensorial effective properties. These tensors can be evaluated through the provided closure problem where the required inputs are the velocity and turbulent viscosity fields that result from the turbulent simulations. Basically, we have developed a method to evaluate Ergun coefficients in a large range of Reynold's number from creeping flow to turbulent flow regimes.

The theory has been successfully validated through 2D and 3D simulations and has been applied to the macro-scale characterization of gas flow through columns equipped with structured packings. We have investigated the dependency of the apparent permeability tensor with the orientation and the magnitude of the flow in a large range of mass flow rates. In the particular case we studied, the flow orientation seems to have a very low impact on the permeability tensor values. The same methodology should be used to characterize effective properties of structured packings with a stronger anisotropic design.

References

[1] B. Antohe, J. Lage, A general two-equation macroscopic turbulence model for incompressible flow in porous media, Int. J. Heat Mass Transfer 40 (13) (1997) 3013–3024.

[2] J. Barrère, Modélisation des écoulements de Stokes et de Navier–Stokes en milieu poreux (Ph.D. thesis), Université de Bordeaux 1, 1990.
[3] R. Billet, M. Schultes, Prediction of mass transfer columns with dumped and arranged packings: updated summary of the calculation method of Billet and Schultes, Chem. Eng. Res. Des. 77 (6) (1999) 498–504.
[4] J.L. Bravo, J.A. Rocha, J.R. Fair, Pressure drop in structured packings, Hydrocarbon process. (1986) 65.
[5] M. Chandesris, A. D'Hueppe, B. Mathieu, D. Jamet, B. Goyeau, Direct numerical simulation of turbulent heat transfer in a fluid-porous domain, Phys. Fluids 25 (12) (2013).
[6] M. Chandesris, D. Jamet, Derivation of jump conditions for the turbulence model at a fluid/porous interface, Int. J. Heat Fluid Flow 30 (2) (2009) 306–318.
[7] M. Chandesris, G. Serre, P. Sagaut, A macroscopic turbulence model for flow in porous media suited for channel, pipe and rod bundle flows, Int. J. Heat Mass Transfer 49 (2006) 2739–2750.
[8] G. Chauveteau, C. Thirriot, Sur les pertes de charge en écoulement laminaire dans quelques géométries simples et dans le milieu poreux, Trieste, 1965, 1–7.
[9] G. Chauveteau, C. Thirriot, Régimes d'écoulement en milieu poreux et limite de la loi de Darcy, La Houille Blanche 2 (1967) 141–148.
[10] M.J. de Lemos, Turbulence in Porous Media: Modelling and Applications, Pergamon, Tarrytown, 2006.
[11] M.J. de Lemos, Turbulence in Porous Media: Modelling and Applications, second ed., Pergamon, Tarrytown, 2012.
[12] M. Drouin, O. Grégoire, O. Simonin, A consistent methodology for the derivation and calibration of a macroscopic turbulence model for flows in porous media, Int. J. Heat Mass Transfer 63 (0) (2013) 401–413.
[13] D.A. Edwards, M. Shapiro, P. Bar-Yoseph, M. Shapira, The influence of reynolds number upon the apparent permeability of spatially periodic arrays of cylinders, Phys. Fluids A: Fluid Dyn. 2 (1) (1990) 45–55.
[14] H. Ene, E. Sanchez-Palencia, Equations et phénomènes de surface pour l'écoulement dans un modèle de milieu poreux, J. Mécanique (1975) 14.
[15] S. Ergun, Fluid flow through packed columns, Chem. Eng. Prog. 48 (2) (1952) 89–94.
[16] P. Forchheimer, Wasserbewegung durch boden, Z. Ver. Deutsch. Ing. 45 (1901) 1782–1788.
[17] D. Getachew, W. Minkowycz, J. Lage, A modified form of the $k-\epsilon$ model for turbulent flows of an incompressible fluid in porous media, Int. J. Heat Mass Transfer 43 (16) (2000) 2909–2915.
[18] S.H. Hosseini, S. Shojaee, G. Ahmadi, M. Zivdar, Computational fluid dynamics studies of dry and wet pressure drops in structured packings, J. Indus. Eng. Chem. (0) (2012).
[19] F. Kuwahara, T. Yamane, A. Nakayama, Large eddy simulation of turbulent flow in porous media, Int. Commun. Heat Mass Transfer 33 (2006) 411–418.
[20] D. Lasseux, A.A.A. Arani, A. Ahmadi, On the stationary macroscopic inertial effects for one phase flow in ordered and disordered porous media, Phys. Fluids 23 (7) (2011) 073103.
[21] B.E. Launder, B.I. Sharma, Application of the energy-dissipation model of turbulence to the calculation of flow near a spinning disc, Lett. Heat Mass Transfer 1 (1974) 131–137.
[22] B. Mahr, D. Mewes, CFD modelling and calculation of dynamic two-phase flow in columns equipped with structured packing, Chem. Eng. Res. Des. 85 (8) (2007) 1112–1122.
[23] C.M. Marle, Ecoulements Monophasiques en Milieu Poreux (1967) 1471–1509.
[24] T. Masuoka, Y. Takatsu, Turbulence model for flow through porous media, Int. J. Heat Mass Transfer 39 (13) (1996) 2803–2809.
[25] F. Menter, T. Esch, Elements of industrial heat transfer predictions, in: COBEM 2001, 16th Brazilian Congress of Mechanical Engineering, 2001.
[26] D. Mewes, T. Loser, M. Millies, Modelling of two-phase flow in packings and monoliths, Chem. Eng. Sci. 54 (21) (1999) 4729–4747.
[27] A. Nakayama, F. Kuwahara, A general macroscopic turbulence model for flows in packed beds, channels, pipes, and rod bundles, J. Fluids Eng. 130 (2008).
[28] A. Nakayama, F. Kuwahara, A macroscopic turbulence model for flow in a porous medium, J. Fluids Eng. 121 (1999) 427–433.
[29] M.K. Nikou, M. Ehsani, Turbulence models application on CFD simulation of hydrodynamics, heat and mass transfer in a structured packing, Int. Commun. Heat Mass Transfer 35 (9) (2008) 1211–1219.
[30] Z. Olujic, M. Jödecke, A. Shilkin, G. Schuch, B. Kaibel, Equipment improvement trends in distillation, Chem. Eng. Process.: Process Intensification 48 (6) (2009) 1089–1104.
[31] Patankar, Numer. Heat Transf. Fluid Flow, Tay, 1980.
[32] M.H. Pedras, M.J. de Lemos, On the definition of turbulent kinetic energy for flow in porous media, Int. Commun. Heat Mass Transfer 27 (2) (2000) 211–220.
[33] M.H.J. Pedras, M.J.S. de Lemos, Macroscopic turbulence modeling for incompressible flow through undeformable porous media, Int. J. Heat Mass Transfer 44 (6) (2001) 1081–1093.
[34] C.F. Petre, F. Larachi, I. Iliuta, B.P.A. Grandjean, Pressure drop through structured packings: breakdown into the contributing mechanisms by cfd modeling, Chem. Eng. Sci. 58 (1) (2003) 163–177.
[35] F. Pinson, O. Grégoire, O. Simonin, $k-\epsilon$ macro-scale modeling of turbulence based on a two scale analysis in porous media, Int. J. Heat Fluid Flow 27 (5) (2006) 955–966 (Special issue of the 6th International Symposium on Engineering Turbulence Modelling and Measurements – ETMM6).
[36] B. Porterie, J.-L. Consalvi, J.-C. Loraud, F. Giroud, C. Picard, Dynamics of wildland fires and their impact on structures, Combust. Flame 149 (3) (2007) 314–328.
[37] M. Quintard, S. Whitaker, Convection, dispersion, and interfacial transport of contaminants: homogeneous porous media, Adv. Water Resour. 17 (4) (1994) 221–239.
[38] M. Quintard, S. Whitaker, Transport in ordered and disordered porous media I: the cellular average and the use of weighting functions, Transp. Porous Media 14 (1994) 163–177, http://dx.doi.org/10.1007/BF00615199.
[39] M. Quintard, S. Whitaker, Transport in ordered and disordered porous media II: generalized volume averaging, Transp. Porous Media 14 (1994) 179–206, http://dx.doi.org/10.1007/BF00615200.
[40] M. Quintard, S. Whitaker, Transport in ordered and disordered porous media III: closure and comparison between theory and experiment, Transp. Porous Media 15 (1994) 31–49, http://dx.doi.org/10.1007/BF01046157.
[41] A. Rafati Saleh, S.H. Hosseini, S. Shojaee, G. Ahmadi, CFD studies of pressure drop and increasing capacity in mellapakplus 752.y structured packing, Chem. Eng. Technol. 34 (9) (2011) 1402–1412. <http://dx.doi.org/10.1002/ceat.201000557>.
[42] L. Raynal, C. Boyer, J.-P. Ballaguet, Liquid holdup and pressure drop determination in structured packing with cfd simulations, Can. J. Chem. Eng. 82 (5) (2004) 871–879.
[43] L. Raynal, A. Royon-Lebeaud, A multi-scale approach for CFD calculations of gas–liquid flow within large size column equipped with structured packing, Chem. Eng. Sci. 62 (24) (2007) 7196–7204 (8th International Conference on Gas–Liquid and Gas–Liquid–Solid Reactor Engineering).
[44] J.A. Rocha, J.L. Bravo, J.R. Fair, Distillation columns containing structured packings: a comprehensive model for their performance. 1. hydraulic models, Ind. Eng. Chem. Res. 32 (4) (1993) 641–651.
[45] W. Said, M. Nemer, D. Clodic, Modeling of dry pressure drop for fully developed gas flow in structured packing using CFD simulations, Chem. Eng. Sci. 66 (10) (2011) 2107–2117.
[46] E. Skjetne, J.-L. Auriault, High-velocity laminar and turbulent flow in porous media, Transp. Porous Media 36 (1999) 131–147, http://dx.doi.org/10.1023/A:1006582211517.
[47] C. Soulaine. Modélisation des écoulements dans les garnissages structurés: de l'échelle du pore à l'échelle de la colonne (Ph.D. thesis), Institut National Polytechnique de Toulouse, 2012.
[48] L. Spiegel, W. Meier, Distillation columns with structured packings in the next decade, Chem. Eng. Res. Des. 81 (1) (2003) 39–47 (International Conference on Distillation and Absorption).
[49] J. Stichlmair, J.L. Bravo, J.R. Fair, General model for prediction of pressure drop and capacity of countercurrent gas/liquid packed columns, Gas Sep. Purif. 3 (1) (1989) 19–28.
[50] F.J. Valdès-Parada, J.A. Ochoa-Tapia, J. Alvarez-Ramirez, Validity of the permeability Carman–Kozeny equation: a volume averaging approach, Phys. A: Stat. Mech. Appl. 388 (6) (2009) 789–798.
[51] S. Whitaker, Flow in porous media I: a theoretical derivation of Darcy's law, Transp. Porous Media 1 (1986) 3–25, http://dx.doi.org/10.1007/BF01036523.
[52] S. Whitaker, The Forchheimer equation: a theoretical development, Transp. Porous Media 25 (1996) 27–61, http://dx.doi.org/10.1007/BF00141261.
[53] S. Whitaker, The Method of Volume Averaging of Theory And Applications of Transport in Porous Media, vol. 13, Kluwer Academic Publishers, 1999.
[54] D.C. Wilcox, Turbulence modeling for CFD, DCW Industrie, Inc, 1994.
[55] J.-C. Wodié, T. Lévy, Correction non-linéaire de la loi de Darcy, C.R. Acad. Sci. Paris 312 (1991) 157–161.